

Production of the charmonium states χ_{c1} and χ_{c2} in proton nucleus interactions at $\sqrt{s} = 41.6$ GeV

I. Abt,²⁴ M. Adams,¹¹ M. Agari,¹⁴ H. Albrecht,¹³ A. Aleksandrov,³⁰ V. Amaral,⁹ A. Amorim,⁹ S. J. Aplin,¹³ V. Aushev,¹⁷ Y. Bagaturia,^{13,37} V. Balagura,²³ M. Bargiotti,⁶ O. Barsukova,¹² J. Bastos,⁹ J. Batista,⁹ C. Bauer,¹⁴ Th. S. Bauer,¹ A. Belkov,^{12,*} Ar. Belkov,¹² I. Belotelov,¹² A. Bertin,⁶ B. Bobchenko,²³ M. Böcker,²⁷ A. Bogatyrev,²³ G. Bohm,³⁰ M. Bräuer,¹⁴ M. Bruinsma,^{29,1} M. Bruschi,⁶ P. Buchholz,²⁷ T. Buran,²⁵ J. Carvalho,⁹ P. Conde,^{2,13} C. Cruse,¹¹ M. Dam,¹⁰ K. M. Danielsen,²⁵ M. Danilov,²³ S. De Castro,⁶ H. Deppe,¹⁵ X. Dong,³ H. B. Dreis,¹⁵ V. Egorytchev,¹³ K. Ehret,¹¹ F. Eisele,¹⁵ D. Emeliyanov,¹³ S. Essenov,²³ L. Fabbri,⁶ P. Faccioli,⁶ M. Feuerstack-Raible,¹⁵ J. Flammer,¹³ B. Fominykh,^{23,*} M. Funcke,¹¹ Ll. Garrido,² A. Gellrich,³⁰ B. Giacobbe,⁶ J. Gläß,²¹ D. Goloubkov,^{13,34} Y. Golubkov,^{13,35} A. Golutvin,²³ I. Golutvin,¹² I. Gorbounov,^{13,27} A. Gorišek,¹⁸ O. Gouchtchine,²³ D. C. Goulart,⁸ S. Gradl,¹⁵ W. Gradl,¹⁵ F. Grimaldi,⁶ J. Groth-Jensen,¹⁰ Yu. Guilitsky,^{23,36} J. D. Hansen,¹⁰ J. M. Hernández,³⁰ W. Hofmann,¹⁴ M. Hohmann,¹³ T. Hott,¹⁵ W. Hulsbergen,¹ U. Husemann,²⁷ O. Igonkina,²³ M. Ispiryan,¹⁶ T. Jagla,¹⁴ C. Jiang,³ H. Kapitza,¹³ S. Karabekyan,²⁶ N. Karpenko,¹² S. Keller,²⁷ J. Kessler,¹⁵ F. Khasanov,²³ Yu. Kiryushin,¹² I. Kisel,²⁴ E. Klinkby,¹⁰ K. T. Knöpfle,¹⁴ H. Kolanoski,⁵ S. Korpar,^{22,18} C. Krauss,¹⁵ P. Kreuzer,^{13,20} P. Krizan,^{19,18} D. Krücker,⁵ S. Kupper,¹⁸ T. Kvaratskheliia,²³ A. Lanyov,¹² K. Lau,¹⁶ B. Lewendel,¹³ T. Lohse,⁵ B. Lomonosov,^{13,33} R. Männer,²¹ R. Mankel,³⁰ S. Masciocchi,¹³ I. Massa,⁶ I. Matchikhilian,²³ G. Medin,⁵ M. Medinnis,¹³ M. Mevius,¹³ A. Michetti,¹³ Yu. Mikhailov,^{23,36} R. Mizuk,²³ R. Muresan,¹⁰ M. zur Nedden,⁵ M. Negodaev,^{13,33} M. Nörenberg,¹³ S. Nowak,³⁰ M. T. Núñez Pardo de Vera,¹³ M. Ouchrif,^{29,1} F. Ould-Saada,²⁵ C. Padilla,¹³ D. Peralta,² R. Pernack,²⁶ R. Pestotnik,¹⁸ B. AA. Petersen,¹⁰ M. Piccinini,⁶ M. A. Pleier,¹⁴ M. Poli,^{6,32} V. Popov,²³ D. Pose,^{12,15} S. Prystupa,¹⁷ V. Pugatch,¹⁷ Y. Pylypchenko,²⁵ J. Pyrlík,¹⁶ K. Reeves,¹⁴ D. Reßing,¹³ H. Rick,¹⁵ I. Riu,¹³ P. Robmann,³¹ I. Rostovtseva,²³ V. Rybnikov,¹³ F. Sánchez,¹⁴ A. Sbrizzi,¹ M. Schmelling,¹⁴ B. Schmidt,¹³ A. Schreiner,³⁰ H. Schröder,²⁶ U. Schwanke,³⁰ A. J. Schwartz,⁸ A. S. Schwarz,¹³ B. Schwenninger,¹¹ B. Schwingenheuer,¹⁴ F. Sciacca,¹⁴ N. Semprini-Cesari,⁶ S. Shuvalov,^{23,5} L. Silva,⁹ L. Sözüer,¹³ S. Solunin,¹² A. Somov,¹³ S. Somov,^{13,34} J. Spengler,¹³ R. Spighi,⁶ A. Spiridonov,^{30,23} A. Stanovnik,^{19,18} M. Starič,¹⁸ C. Stegmann,⁵ H. S. Subramania,¹⁶ M. Symalla,^{13,11} I. Tikhomirov,²³ M. Titov,²³ I. Tsakov,²⁸ U. Uwer,¹⁵ C. van Eldik,^{13,11} Yu. Vassiliev,¹⁷ M. Villa,⁶ A. Vitale,^{6,7,*} I. Vukotic,^{5,30} H. Wahlberg,²⁹ A. H. Walenta,²⁷ M. Walter,³⁰ J. J. Wang,⁴ D. Wegener,¹¹ U. Werthenbach,²⁷ H. Wolters,⁹ R. Wurth,¹³ A. Wurz,²¹ S. Xella-Hansen,¹⁰ Yu. Zaitsev,²³ M. Zavertyaev,^{13,14,33} T. Zeuner,^{13,27} A. Zhelezov,²³ Z. Zheng,³ R. Zimmermann,²⁶ T. Živko,¹⁸ and A. Zoccoli⁶

(The HERA-B Collaboration)

¹NIKHEF, 1009 DB Amsterdam, The Netherlands²Department ECM, Faculty of Physics, University of Barcelona, E-08028 Barcelona, Spain³Institute for High Energy Physics, Beijing 100039, P.R. China⁴Institute of Engineering Physics, Tsinghua University, Beijing 100084, P.R. China⁵Institut für Physik, Humboldt-Universität zu Berlin, D-12489 Berlin, Germany⁶Dipartimento di Fisica dell'Università di Bologna and INFN Sezione di Bologna, I-40126 Bologna, Italy⁷Fondazione Giuseppe Occhialini, I-61034 Fossombrone (Pesaro Urbino), Italy⁸Department of Physics, University of Cincinnati, Cincinnati, Ohio 45221, USA⁹LIP Coimbra, P-3004-516 Coimbra, Portugal¹⁰Niels Bohr Institutet, DK 2100 Copenhagen, Denmark¹¹Institut für Physik, Universität Dortmund, D-44221 Dortmund, Germany¹²Joint Institute for Nuclear Research Dubna, 141980 Dubna, Moscow, Russia¹³DESY, D-22603 Hamburg, Germany¹⁴Max-Planck-Institut für Kernphysik, D-69117 Heidelberg, Germany¹⁵Physikalisches Institut, Universität Heidelberg, D-69120 Heidelberg, Germany¹⁶Department of Physics, University of Houston, Houston, Texas 77204, USA¹⁷Institute for Nuclear Research, Ukrainian Academy of Science, 03680 Kiev, Ukraine¹⁸J. Stefan Institute, 1001 Ljubljana, Slovenia¹⁹University of Ljubljana, 1001 Ljubljana, Slovenia²⁰University of California, Los Angeles, California 90024, USA²¹Lehrstuhl für Informatik V, Universität Mannheim, D-68131 Mannheim, Germany²²University of Maribor, 2000 Maribor, Slovenia²³Institute of Theoretical and Experimental Physics, 117218 Moscow, Russia²⁴Max-Planck-Institut für Physik, Werner-Heisenberg-Institut, D-80805 München, Germany²⁵Department of Physics, University of Oslo, N-0316 Oslo, Norway

²⁶*Fachbereich Physik, Universität Rostock, D-18051 Rostock, Germany*²⁷*Fachbereich Physik, Universität Siegen, D-57068 Siegen, Germany*²⁸*INRNE-BAS, Sofia, Bulgaria*²⁹*Universiteit Utrecht/NIKHEF, 3584 CB Utrecht, The Netherlands*³⁰*DESY, D-15738 Zeuthen, Germany*³¹*Physik-Institut, Universität Zürich, CH-8057 Zürich, Switzerland*³²*Dipartimento di Energetica dell' Università di Firenze and INFN Sezione di Bologna, Italy*³³*P.N. Lebedev Physical Institute, 117924 Moscow B-333, Russia*³⁴*Moscow Physical Engineering Institute, 115409 Moscow, Russia*³⁵*Moscow State University, 119992 Moscow, Russia*³⁶*Institute for High Energy Physics, Protvino, Russia*³⁷*High Energy Physics Institute, 380086 Tbilisi, Georgia*

(Received 14 July 2008; published 13 January 2009)

A measurement of the ratio $R_{\chi_c} = (\chi_c \rightarrow J/\psi + \gamma)/J/\psi$ in pC , pTi , and pW interactions at 920 GeV/c ($\sqrt{s} = 41.6$ GeV) in the Feynman-x range $-0.35 < x_F^{J/\psi} < 0.15$ is presented. Both $\mu^+ \mu^-$ and $e^+ e^- J/\psi$ decay channels are observed with an overall statistics of about 15 000 χ_c events, which is by far the largest available sample in pA collisions. The result is $R_{\chi_c} = 0.188 \pm 0.013_{\text{stat}}^{+0.024}_{-0.022\text{sys}}$ averaged over the different materials, when no J/ψ and χ_c polarizations are considered. The χ_{c1} to χ_{c2} production ratio $R_{12} = R_{\chi_{c1}}/R_{\chi_{c2}}$ is measured to be 1.02 ± 0.40 , leading to a cross section ratio $\frac{\sigma(\chi_{c1})}{\sigma(\chi_{c2})} = 0.57 \pm 0.23$. The dependence of R_{χ_c} on the Feynman-x of the J/ψ , $x_F^{J/\psi}$, and its transverse momentum, $p_T^{J/\psi}$, is studied, as well as its dependence on the atomic number, A , of the target. For the first time, an extensive study of possible biases on R_{χ_c} and R_{12} due to the dependence of acceptance on the polarization states of J/ψ and χ_c is performed. By varying the polarization parameter, λ_{obs} , of all produced J/ψ 's by two sigma around the value measured by HERA-B, and considering the maximum variation due to the possible χ_{c1} and χ_{c2} polarizations, it is shown that R_{χ_c} could change by a factor between 1.02 and 1.21 and R_{12} by a factor between 0.89 and 1.16.

DOI: 10.1103/PhysRevD.79.012001

PACS numbers: 13.20.Gd, 13.85.-t, 24.85.+p, 13.88.+e

I. INTRODUCTION

Since the discovery of charmonium more than 30 years ago, its production in hadronic collisions has attracted considerable theoretical and experimental interest for a variety of reasons. In particular, the question of the production mechanism, which requires an understanding of the hadronization process in the nonperturbative regime and, in addition, the influence of nuclear matter, are of particular importance, since the suppression of J/ψ production has been considered as a possible indicator of the quark-gluon plasma [1].

The theoretical treatment of quarkonium production is usually broken into two steps: the creation of a heavy quark pair in interactions of the colliding partons, calculable by means of perturbative QCD, and the transition to a bound state, involving poorly understood nonperturbative processes and even more problematic nuclear effects. A variety of approaches have been developed to describe quarkonium production such as the Color Evaporation Model (CEM) [2], the Color Singlet Model (CSM) [3], and nonrelativistic QCD (NRQCD) [4]. A measurement of the fraction of J/ψ coming from the decay of other charmonium states (feeddown) provides useful tests of the model predictions. While a rather rich sample of data on

J/ψ production exists, the available data on the production rates, or even the experimentally simpler fractional production rates of the other charmonium states suffer from imprecision. Moreover, very little experimental information is available on the possible polarization of the produced charmonium states.

In this paper we report on the production of the charmonium states χ_{c1} and χ_{c2} in collisions of a 920 GeV proton beam with nuclear targets. The χ_c mesons are identified via their radiative decay into J/ψ mesons, which in turn are decaying into lepton pairs. The production and decay chain is

$$pA \rightarrow \chi_c + X; \quad \chi_c \rightarrow \gamma J/\psi \rightarrow \gamma l^+ l^- \quad (l = e, \mu). \quad (1)$$

To minimize systematic uncertainties the χ_c rates are normalized to the total production rate of J/ψ . We define R_{χ_c} , the fraction of J/ψ originating from radiative χ_c decays

$$R_{\chi_c} = \frac{\sum_{i=1}^2 \sigma(\chi_{ci}) \text{Br}(\chi_{ci} \rightarrow J/\psi \gamma)}{\sigma(J/\psi)}, \quad (2)$$

where $\text{Br}(\chi_{ci} \rightarrow J/\psi \gamma)$ are the branching ratios for the different $\chi_{ci} \rightarrow J/\psi \gamma$ decays, $\sigma(\chi_{ci})$ are their production cross sections per nucleon, and $\sigma(J/\psi)$ is the total J/ψ production cross section per nucleon. In Table I, the main properties of the three χ_c states (χ_{c0} , χ_{c1} and χ_{c2}) are

*Deceased.

TABLE I. Properties of the three χ_c states [5].

State	$I^G(J^{PC})$	Mass (MeV/ c^2)	Width (MeV/ c^2)	BR($\rightarrow J/\psi\gamma$) (%)
χ_{c0}	$0^+(0^{++})$	3414.76 ± 0.35	10.4 ± 0.7	(1.30 ± 0.11)
χ_{c1}	$0^+(1^{++})$	3510.66 ± 0.07	0.89 ± 0.05	(35.6 ± 1.9)
χ_{c2}	$0^+(2^{++})$	3556.20 ± 0.09	2.06 ± 0.12	(20.2 ± 1.0)

reported. Because of the negligible $\chi_{c0} \rightarrow J/\psi\gamma$ branching ratio, we limit our study to χ_{c1} and χ_{c2} production.

In Sec. II, an overview of the physics motivations for our measurement is given together with a survey of the existing experimental results. In Sec. III, the experiment and the data taking conditions are described, and in Sec. IV, the principle of the measurement is explained. The simulation used for evaluating detection efficiencies and the measurements in the muon and electron decay channels are described in Secs. V, VIA, and VIB, respectively. In Sec. VII, the effect of possible J/ψ and χ_c polarizations (not directly measured in this analysis) on R_{χ_c} and $R_{12} = R_{\chi_{c1}}/R_{\chi_{c2}}$ is discussed. A discussion of systematic uncertainties and the final result are given in Secs. VIII and IX, respectively.

II. χ_c PRODUCTION

A. QCD models of charmonium production

In the CEM, charmonium production is described as the creation of $c\bar{c}$ pairs with an invariant mass below the $D\bar{D}$ threshold. Their hadronization is mediated by the emission of soft gluons that do not significantly alter the kinematics of the $c\bar{c}$ system. The fraction of below-threshold $c\bar{c}$ pairs hadronizing into each of the individual charmonium states is predicted to be independent of the initial state particles and collision energy. Moreover, the differential distributions of the various charmonium states with respect to x_F and p_T are predicted to be the same [6]. Most experiments measuring R_{χ_c} in proton and pion-induced interactions [7–22] provide compatible results with the predicted value $R_{\chi_c} \approx 0.4$ [6]. The assumption of the universality of charmonium hadronization implies that the value of R_{χ_c} should be independent of the kinematic variables x_F and p_T of the produced charmonium state [6] (x_F is the Feynman variable in the nucleon-nucleon center-of-mass system; p_T is the transverse momentum relative to the incoming beam).

In the CSM, the quark pair is created in a hard scattering reaction as a color singlet (CS) with the same quantum numbers as the final quarkonium. Since two gluons can form a colorless C-even state, such as the χ_c states, at least three gluons are needed to form a colorless C-odd state, such as the ψ states, ψ production in this model is suppressed by an additional factor α_s . As a result, the J/ψ production rate should be dominated by feeddown from

radiative χ_c decays, and R_{χ_c} is predicted to be close to 1. Most of the proton induced χ_c measurements are in disagreement with this assumption [7–15].

In response to the disagreement between the CSM and measurements in most charmonium production features [23], a more generalized perturbative QCD approach for charmonium production, “nonrelativistic QCD” (NRQCD), was developed, which includes not only $c\bar{c}$ pairs produced as color singlets but also as color octets (CO). The CO states subsequently evolve into the observed charmonium by soft gluon emission. At the HERA-B beam energy of 920 GeV, the dominant production process is gg fusion, which contributes both to CO and CS states. Therefore, χ_c production dominates the CS part of J/ψ production, while direct J/ψ and J/ψ from $\psi(2S)$ decay are produced via CO states. The predicted ratio $R_{\chi_c} \approx 0.3$ [6] is in agreement with most of the existing measurements in proton induced interactions [7–15]. NRQCD predicts only small differences in the differential cross sections of the different charmonium states as a function of x_F , mostly at large values of x_F . More visible differences can arise when considering nuclear-matter effects (A-dependence) due to the differing absorption probabilities of the various charmonium and precharmonium states in nuclei [6].

B. Interactions with nucleons and A-dependence

The CEM model and NRQCD differ in their predictions of the suppression of the charmonium production rate per nucleon in interactions with heavy nuclei compared with interactions with single proton targets. Suppression can occur in interactions of the generated $c\bar{c}$ quarks with nuclear matter, which could lead to an x_F dependence: for $x_F > 0$, the formation length of the final charmonium state exceeds the size of the nucleus, while for $x_F < 0$, an increasingly larger fraction is formed already inside the nucleus. In the context of the CEM, only one proto-charmonium state exists and thus for $x_F > 0$, the differences in suppression between J/ψ , $\psi(2S)$ and the χ_c states should be small. For $x_F < 0$, the χ_c and $\psi(2S)$ states should be more suppressed than the J/ψ due to their larger interaction cross sections [6,24]. In the context of NRQCD, substantial differences in the suppression of the various charmonium states are expected even for $x_F > 0$, since the wave function of the CO states extends over a much larger distance, and the resulting interaction cross section is considerably larger than that of the CS states [6].

C. R_{χ_c} and the quark-gluon plasma

The so-called ‘‘anomalous’’ suppression of J/ψ has been proposed as a possible indicator of the formation of a quark-gluon plasma [1], and such suppression has subsequently been reported by several experiments [25–27]. Nevertheless, the conclusion that the reported suppression is indeed anomalous is contingent on the full understanding of normal suppression mechanisms, i.e. those existing in the absence of a quark-gluon plasma as is expected to be the case in proton-nucleus reactions. In this respect, the measurement of the fraction of J/ψ arising from feeddown decays (χ_c and $\psi(2S)$) is important, since the anomalous suppression is expected to be sensitive to the mass and

binding energy of the different charmonium states. Directly produced J/ψ survive in the quark-gluon plasma up to about $1.5T_c$ [28], T_c being the critical temperature, while χ_c and $\psi(2S)$ states dissociate just above T_c . Thus, several drops in the distribution of charmonium survival probability as a function of the temperature are expected, with the size of the drops dependent on the fractions R_{χ_c} and $R_{\psi(2S)}$ ($R_{\psi(2S)} = \frac{\sigma(\psi(2S))\text{Br}(\psi(2S)\rightarrow J/\psi X)}{\sigma(J/\psi)}$). Experimentally, only the first drop has been reported [25–27], and is interpreted as indicating the dissociation of χ_c and $\psi(2S)$. Several models attempt to describe the totality of experimental data on J/ψ suppression. They generally assume $R_{\chi_c} \sim 0.3$ and $R_{\psi(2S)} \sim 0.1$. Nevertheless, all the proposed

TABLE II. Previous R_{χ_c} measurements in hadronic collisions. Symbols: γ detection ($d = \text{direct}$, $c = \gamma\text{-conversion}$). $\chi_{c1}\text{-}\chi_{c2}$ separation ($y = \text{yes}$, $n = \text{no}$, $f = \text{with 2-states fit}$).

Exp.	beam/target	\sqrt{s} GeV	l^+l^-	γ det.	ϵ_γ %	x_F	p_T GeV/ c	E_γ cut GeV	$N_{J/\psi}$	N_{χ_c}	χ_{ci} sep.
R806 [7]	pp	$\langle 55 \rangle$	e^+e^-	d				>0.4	658	31 ± 11	n
R702 [8]	pp	52.4,62.7	e^+e^-	d			<3	0.4–0.6	975		n
R806 [9]	pp	62	e^+e^-	d			<5	>0.4			n
E610 [10]	$p\text{Be}$	19.4,21.7	$\mu^+\mu^-$	d	16	0.1–0.7	<2	3–50	157 ± 17	11.8 ± 5.4	f
E705 [11]	$p\text{Li}$	23.8	$\mu^+\mu^-$	d	27	–0.1–0.5	0.–0.4	>1.0	6090 ± 90	250 ± 35	f
E771 [13]	$p\text{Si}$	38.8	e^+e^-	c	0.8	>0.0		0.25–0.7	$11\,660 \pm 139$	66	y
HERA-B [15]	$p\text{C, Ti}$	41.6	$\{\mu^+\mu^-\}$	d	30	–0.25–0.15		$E_T > 1.0$	4420 ± 100	370 ± 74	n
CDF [12],[14]	$p\bar{p}$	1800	$\mu^+\mu^-$	$\{d^c\}$	$\{15\}$		>4.0	>1.0	$\{88\,000\}$ $\{32\,642 \pm 185\}$	$\{119 \pm 14\}$ $\{1230 \pm 72\}$	$\{n\}$
E369 [16]	$\pi^-\text{Be, } p$	20.2	$\mu^+\mu^-$	d		0–0.8	<3	<5	160	17.2 ± 6.6	n
WA11 [17]	$\pi^-\text{Be}$	18.7	$\mu^+\mu^-$	c	1				44750	157	y
IHEP140 [18]	π^-p	8.6	e^+e^-	d		>0.4	<2	>2	120	10	n
E673 [19]	$\pi^-\text{Be}$	20.6	$\mu^+\mu^-$	d	21			10–25	1056 ± 36	84 ± 15	n
E610 [20]	$\pi^-\text{Be}$	18.9	$\mu^+\mu^-$	d	19	0.1–0.7	<2	3–50	908 ± 41	53.6 ± 17.1	f
E705 [21]	$\{\pi^- - \text{Li}\}$	23.8	$\mu^+\mu^-$	d	27				$\{5560 \pm 90\}$ $\{12\,470 \pm 160\}$	$\{300 \pm 35\}$ $\{590 \pm 50\}$	n
E672/706 [22]	$\pi^-\text{Be}$	31.1	$\mu^+\mu^-$	$\{d^c\}$	$\{11\}$ $\{12\}$	0.1–0.8		>10	7750 ± 110	$\{379 \pm 66\}$ $\{105 \pm 18\}$	$\{f\}$ $\{y\}$

TABLE III. R_{χ_c} , $\frac{\sigma(\chi_{c1})}{\sigma(\chi_{c2})}$, $\sigma(\chi_{c1})$ and $\sigma(\chi_{c2})$ results in hadronic collisions. Statistical and systematic uncertainties are shown in brackets (less significant digits). See text for an explanation of the updated values.

Exp.	Measured values				Updated values			
	R_{χ_c}	$\frac{\sigma(\chi_{c1})}{\sigma(\chi_{c2})}$	$\sigma(\chi_{c1})$ (nb/n)	$\sigma(\chi_{c2})$ (nb/n)	R_{χ_c}	$\frac{\sigma(\chi_{c1})}{\sigma(\chi_{c2})}$	$\sigma(\chi_{c1})$ (nb/n)	$\sigma(\chi_{c2})$ (nb/n)
[7]	0.43 ± 0.21				0.43 ± 0.21			
[8]	$0.15^{+0.10}_{-0.15}$				$0.15^{+0.10}_{-0.15}$			
[9]	0.47(8)				0.47(8)			
[10]	0.47(23)	0.24(28)	64(81)	268(136)	0.47(23)	0.24(28)	39(49)	162(81)
[11]	0.30(4)	0.08(25)(15)	31(62)(3)	364(124)(36)	0.30(4)	0.09(29)(17)	24(48)(2)	244(83)(16)
[13]	0.77(30)(15)	0.53(20)(7)	526(138)(64)	996(286)(134)	0.76(29)(16)	0.61(24)(4)	488(128)(56)	805(231)(92)
[15]	0.32(6)(4)				0.32(6)(4)			
[12]	0.297(17)(57)	1.04(29)(12)			0.297(17)(57)	1.19(33)(14)		
[16]	0.70(28)				0.70(28)			
[17]	0.30(5)	0.68(28)	65(18)	96(29)	0.30(5)	0.79(28)	58(13)	74(19)
[18]	0.44(16)	1(fix)	28(10)	28(10)	0.44(16)	1(fix)	22(8)	22(8)
[19]	0.37(9)	1.12(42)			0.37(9)	1.11(41)		
[20]	0.31(10)	0.96(64)	130(56)	134(64)	0.31(10)	0.98(74)	102(43)	104(49)
[21]	0.40(4)				0.40(4)			
[21]	0.37(3)	0.70(15)	131(17)	189(31)	0.37(3)	0.80(16)	101(13)	126(19)
[22]	0.443(41)(35)	0.57(16)	464(87)	815(168)	0.443(41)(35)	0.65(18)	356(66)	544(107)

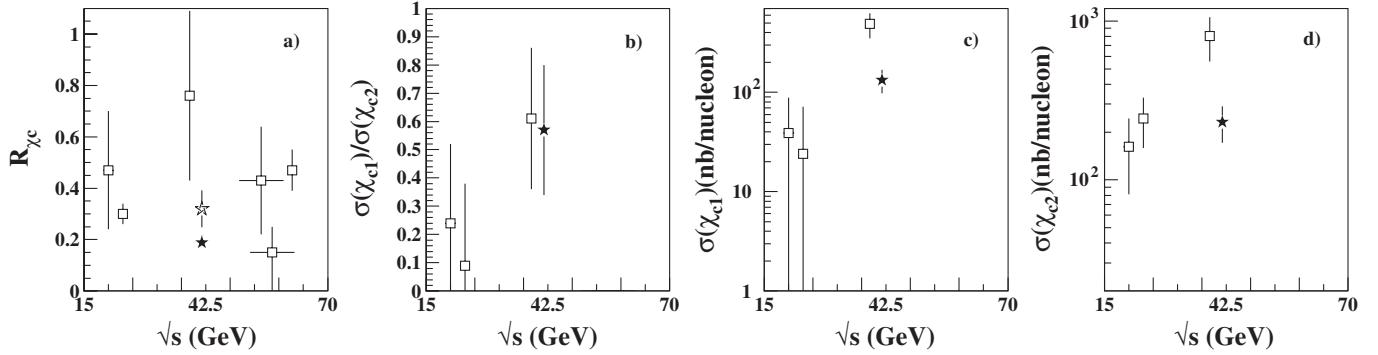


FIG. 1. Summary of experimental results on R_{χ_c} (a), $\frac{\sigma(\chi_{c1})}{\sigma(\chi_{c2})}$ (b), $\sigma(\chi_{c1})$ (c) and $\sigma(\chi_{c2})$ (d) in pN interactions. HERA-B results: open star (old), full star (new).

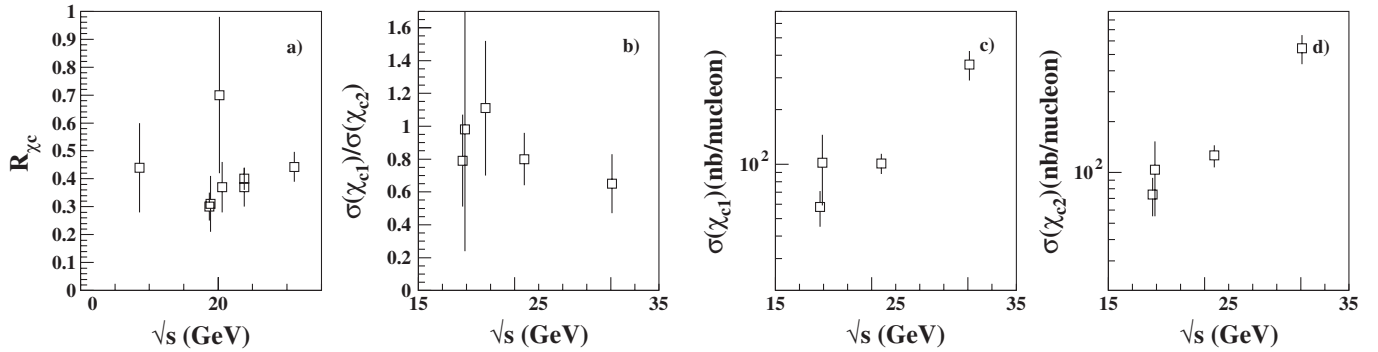


FIG. 2. Summary of experimental results on R_{χ_c} (a), $\frac{\sigma(\chi_{c1})}{\sigma(\chi_{c2})}$ (b), $\sigma(\chi_{c1})$ (c), and $\sigma(\chi_{c2})$ (d) in πN interactions.

models fail to simultaneously describe all the existing data, as they all overestimate the suppression unless other effects, such as J/ψ regeneration, are assumed to describe the RHIC data [28]. From the value of R_{χ_c} shown in Sec. IX and the result from [29], $R_{\psi(2S)} \approx 7\%$, $R_{\chi_c} + R_{\psi(2S)} \approx 0.27$, which is lower than generally assumed.

D. Previous measurements

The production of χ_c has been measured both in proton- and pion-induced reactions on various nuclear targets and in pp and $p\bar{p}$ interactions [7–22]. Table II lists all the published measurements of χ_c production in hadronic interactions and reports their most relevant features. From this table some observations can be made:

- (i) All fixed-target measurements are based on at most a few hundreds χ_c ;
- (ii) All experiments observe only one of the two J/ψ decay channels (e^+e^- or $\mu^+\mu^-$);
- (iii) The photon efficiency never exceeds 30%;
- (iv) Most measurements are performed in the positive x_F range.

Table III shows the measured values of R_{χ_c} and/or of the χ_c cross sections separately for proton and pion-induced reactions. The values shown in Figs. 1 and 2 have been updated using the current PDG values [5] for the χ_c and

J/ψ decay branching ratios, and the J/ψ cross sections obtained from [30].

The available data scatter strongly, well beyond their respective uncertainties, and no energy dependence is discernible. The proton data seem to favor a value $R_{\chi_c} \sim 0.3$, supporting the prediction of NRQCD, but the quality of the available data does not allow a firm conclusion.

III. THE EXPERIMENT AND THE DATA SAMPLE

The HERA-B detector [31] was a forward magnetic spectrometer used to study the interactions of the 920 GeV proton beam ($\sqrt{s} = 41.6$ GeV) of the HERA accelerator on a variety of nuclear targets. The detector components relevant for this analysis are the wire target system [32], which could be dynamically positioned in the halo of the proton beam, the silicon vertex detector [33], the dipole magnet of 2.13 Tm, the drift-tube Tracking System (OTR) [34], the Ring Imaging Cherenkov Counter [35], the sampling Electromagnetic Calorimeter (ECAL) [36], and the muon detector [37].

The data sample of about 160×10^6 events used for this analysis was acquired at an interaction rate of about 5 MHz with a dedicated dilepton trigger [38] in order to select both $J/\psi \rightarrow e^+e^-$ and $J/\psi \rightarrow \mu^+\mu^-$ final states. In total about 300 000 J/ψ were reconstructed, distributed almost equally in the two decay channels. Nine different wire

configurations were used, both in single and double wire runs. The wire materials used were carbon (C, $\approx 64\%$ of the full statistics), tungsten (W, $\approx 31\%$), and titanium (Ti, $\approx 5\%$). Continuous online monitoring ensured stable running conditions, and further offline data quality checks were applied to select only runs with properly functioning detector and trigger components.

IV. EXPERIMENTAL METHOD

R_{χ_c} is defined in Eq. (2). The quantity to be measured is

$$R_{\chi_c} = \frac{\frac{N_{\chi_{c1}} \cdot \varepsilon_{J/\psi}^{\text{dir}}}{\varepsilon_{J/\psi}^{\chi_{c1}} \cdot \varepsilon_{\gamma}^{\chi_{c1}}} + \frac{N_{\chi_{c2}} \cdot \varepsilon_{J/\psi}^{\text{dir}}}{\varepsilon_{J/\psi}^{\chi_{c2}} \cdot \varepsilon_{\gamma}^{\chi_{c2}}}}{N_{J/\psi} + \frac{N_{\chi_{c1}}}{\varepsilon_{\gamma}^{\chi_{c1}}} \cdot \left(\frac{\varepsilon_{J/\psi}^{\text{dir}}}{\varepsilon_{J/\psi}^{\chi_{c1}}} - 1 \right) + \frac{N_{\chi_{c2}}}{\varepsilon_{\gamma}^{\chi_{c2}}} \cdot \left(\frac{\varepsilon_{J/\psi}^{\text{dir}}}{\varepsilon_{J/\psi}^{\chi_{c2}}} - 1 \right)}, \quad (3)$$

where $N_{J/\psi}$ is the total number of observed J/ψ 's, $N_{\chi_{c1}}$ ($N_{\chi_{c2}}$) is the number of counted χ_{c1} 's (χ_{c2} 's), $\varepsilon_{J/\psi}^{\text{dir}}$ is the direct J/ψ total detection efficiency, including trigger losses, reconstruction and cut selection, $\varepsilon_{J/\psi}^{\chi_{c1}}$ ($\varepsilon_{J/\psi}^{\chi_{c2}}$) is the total detection efficiency for J/ψ coming from χ_{c1} (χ_{c2}) decay, and $\varepsilon_{\gamma}^{\chi_{c1}}$ ($\varepsilon_{\gamma}^{\chi_{c2}}$) is the identification efficiency of the photon from χ_{c1} (χ_{c2}) decay for events with identified J/ψ 's. The measurement method consists of evaluating $N_{J/\psi}$ by analysis of the dilepton invariant mass spectra and $N_{\chi_{c1}}$, $N_{\chi_{c2}}$ by analysis of the J/ψ - γ invariant mass spectra, for events with selected J/ψ candidates. The efficiency terms in Eq. (3) are extracted from the Monte Carlo (MC) simulation.

The production ratio of the two states can be determined using

$$R_{12} = \frac{R_{\chi_{c1}}}{R_{\chi_{c2}}} = \frac{N_{\chi_{c1}}}{N_{\chi_{c2}}} \cdot \frac{\varepsilon_{J/\psi}^{\chi_{c2}} \cdot \varepsilon_{\gamma}^{\chi_{c2}}}{\varepsilon_{J/\psi}^{\chi_{c1}} \cdot \varepsilon_{\gamma}^{\chi_{c1}}}, \quad (4)$$

(where $R_{\chi_{c1}} + R_{\chi_{c2}} = R_{\chi_c}$) and the production cross section ratio can be evaluated using

$$\frac{\sigma(\chi_{c1})}{\sigma(\chi_{c2})} = R_{12} \frac{\text{Br}(\chi_{c2} \rightarrow J/\psi \gamma)}{\text{Br}(\chi_{c1} \rightarrow J/\psi \gamma)}. \quad (5)$$

In order to perform an internally consistent analysis, the same procedure and cuts are applied to both the e^+e^- and $\mu^+\mu^-$ channels except for the lepton particle identification (PID) requirements.

A. J/ψ selection

Leptons from J/ψ decay are selected from the triggered tracks, refitted using offline alignment constants and taking into account multiple scattering when extrapolating to the target. A χ^2 probability of the track fit $>0.3\%$ is required. Additional PID cuts are applied depending on the lepton channel.

In the muon channel, a muon likelihood is constructed from information in the muon detector and is required to be greater than 5%, and a kaon likelihood is constructed from

Ring Imaging Cherenkov Counter information and required to be less than 99%.

In the electron channel, a more complex set of PID cuts is needed. First, the calorimeter is searched for a cluster consistent with having been caused by a Bremsstrahlung photon emitted in front of the magnet [36]. Since the presence of such a cluster very effectively identifies electrons, the cut values used for the remaining two particle identification criteria can be substantially relaxed when such a Bremsstrahlung cluster is found. The additional two criteria are a more restrictive matching requirement between the OTR track of the electron candidate and its corresponding ECAL cluster, and a requirement that the track momentum be consistent with the deposited calorimeter energy.

Once opposite sign lepton candidates ($\mu^+\mu^-$ or e^+e^-) are selected, their common vertex is fitted, and the χ^2 probability of the fit is required to be greater than 1%. In a few percent of the events, more than one dilepton combination pass all cuts, in which case only the one with the lowest product of track fit χ^2 is retained. Finally, the invariant mass of the dilepton pair is calculated and required to be within 2σ of the nominal J/ψ mass, with $\sigma = 36 \text{ MeV}/c^2$ in the muon channel and $64 \text{ MeV}/c^2$ in the electron channel.

B. Mass difference plot

The next step after J/ψ selection is the identification of suitable photon candidates. A photon is defined as a reconstructed ECAL cluster [39] with at least three contiguous hit cells. The cluster energy E_{γ} is required to be at least 0.3 GeV, and the cluster transverse energy E_T^{γ} is required to be at least 0.2 GeV for an optimal cluster reconstruction. Furthermore, the ECAL cell with the highest energy deposit of the cluster is required to contain at least 80% of the total cluster energy in order to provide some discrimination against showering hadrons. Clusters that match reconstructed tracks are excluded unless the matching track is formed only from hits behind the magnet and point to the selected dilepton vertex. Such tracks are mainly from conversions of event-related photons behind the magnet. Finally, because of high background near the proton beam pipe, clusters in an elliptic region around the pipe ($\sqrt{x_{\text{clust}}^2/4 + y_{\text{clust}}^2} < 22 \text{ cm}$, where x_{clust} and y_{clust} are the horizontal and vertical positions of the cluster with respect to the beam) are excluded.

Since a photon from a χ_c decay cannot be distinguished from the others in the event (on average ~ 20), the combinatorial background to the χ_c signal is very large, as will be shown in Sec. IV C.

To largely eliminate the uncertainty due to dilepton mass resolution, the analysis is performed using the mass difference $\Delta M = M(J/\psi \gamma) - M(J/\psi)$. The dominant contribution to the mass difference resolution is the intrinsic photon energy resolution determined by the ECAL.

C. Background description

The analysis crucially depends on the background shape being correctly described. We distinguish between ‘‘physical’’ backgrounds (due to the decay of heavier states, which include a J/ψ and one or more photons in their decay products) and ‘‘combinatorial’’ background (due to photons from the event combined with dileptons, which share no parent resonance). The combinatorial background by far dominates. The only significant physical background comes from $\psi(2S) \rightarrow J/\psi \pi^0 \pi^0$, which contributes at the level of $\approx 15\%$ of the χ_c rate but with a rather flat distribution in the ΔM spectrum. The shape of this background is estimated from Monte Carlo and subtracted after proper normalization.

A ‘‘mixed event’’ (ME) procedure is adopted for modeling the combinatorial background: a J/ψ candidate from one event (‘‘event A’’) is mixed with the photons of several (≈ 20) other selected events (which we all call ‘‘event B’’). Event B is required to have the same neutral cluster multiplicity as event A to ensure similar photon energy spectra. Furthermore, the angular difference between the vector sums of transverse momenta of all photons in event A and event B is required to be no more than $2\pi/20$ to ensure the events to be kinematically similar and thus to have similar acceptance.

Extensive tests, both with Monte Carlo and the data itself, were performed to verify the ME procedure. For example, using the data, the combination of photons with l^+l^- pairs in the J/ψ side bands (defined as the dilepton mass intervals outside 3σ of the nominal J/ψ mass, see Sec. IVA) in the SE (‘‘same event’’) and with l^+l^- pairs inside the J/ψ mass window in the ME spectra show no reflection of the χ_c peak, and the SE over ME ratio for these events is found to be flat. The normalization of the ME spectrum is incorporated into the fit of the ΔM spectrum as a free parameter (see Sec. VIB).

V. THE MONTE CARLO SIMULATION

A. Event generator and detector simulation

In the HERA-B Monte Carlo, the basic process $pN \rightarrow Q\bar{Q}X$ is simulated, first, by generating the heavy quarks ($Q\bar{Q}$), including hadronization, with PYTHIA 5.7 [40]; secondly, the energy of the remaining part of the process (X) is given as an input to FRITIOF [41], which is used to simulate the interactions inside the nucleus. PYTHIA describes by default the charmonium production based on the color singlet model. Further color singlet and color octet processes were therefore added, according to the NRQCD approach [15]. Differing kinematic distributions for directly produced J/ψ and J/ψ from feeddown decays generated according to this model result in only an insignificant difference in the acceptances: $\sim 78.3\%$ for direct J/ψ and $\sim 77.6\%$ for J/ψ from both χ_{c1} and χ_{c2} .

In the simulation, both direct J/ψ and χ_c states are generated with no polarization, and all results are given

under this assumption. The effects of J/ψ and χ_c polarization are discussed and treated separately (see Sec. VII).

The detector response is simulated using GEANT 3.21 [42] and includes individual detector channel resolutions, noise, efficiencies, and calibration precision. The second level trigger algorithm is applied to the simulated detector hits, and the first level trigger efficiency is taken from an efficiency map obtained from the data itself. The generated Monte Carlo is reconstructed with the same package used for reconstructing the data, and the same analysis cuts are applied to the MC and the data.

In order to check the MC material description, which influences the photon efficiency determination, three different studies were performed by using the Bremsstrahlung tag [36], the π^0 signal (where the decay photons are seen as neutral clusters or as converted photons), and the converted photons (see Sec. VB and VIII).

The predicted resolution of the χ_{c1} and χ_{c2} states is found to be ~ 0.032 GeV/ c^2 , in agreement with real data (see Sec. VIB).

B. J/ψ and photon efficiency

According to Eq. (3), the ratios of efficiencies for J/ψ coming from the decay of the χ_c states to that of directly produced J/ψ are needed. These ratios are estimated from MC, and the values obtained are reported in Table IV. As can be seen from the table, these ratios are independent of target, decay channel, and χ_c state, within the errors.

The photon detection efficiencies are also evaluated with the MC although an additional correction factor derived from the data was found to be needed, as will be discussed below. For the efficiency evaluation, the same analysis as for the data is performed, but the photon from the χ_c decay is selected using MC generation information and checked for acceptance after all cuts are applied. The alternative of extracting the number of χ_c 's from the MC using the ME background subtraction applied to the data, and thus inferring the photon efficiency without recourse to the MC generation information, was found to give a compatible efficiency, but with lower precision.

The MC estimate for photon detection efficiency was checked by comparing the efficiency derived from MC with that obtained from data for the detection by the

TABLE IV. The ratio of efficiencies for detection of directly produced J/ψ 's to that of J/ψ 's coming from χ_{c1} and χ_{c2} decay. The efficiencies for $\mu^+\mu^-$ and e^+e^- channels and for each target material are given separately.

Mat.	$\frac{\epsilon_{J/\psi}^{\text{dir}}}{\epsilon_{\chi_{c1}}^{\text{dir}}}$	$\mu^+\mu^-$ $\frac{\epsilon_{J/\psi}^{\text{dir}}}{\epsilon_{\chi_{c2}}^{\text{dir}}}$	$\frac{\epsilon_{J/\psi}^{\text{dir}}}{\epsilon_{\chi_{c1}}^{\text{dir}}}$	e^+e^- $\frac{\epsilon_{J/\psi}^{\text{dir}}}{\epsilon_{\chi_{c2}}^{\text{dir}}}$
C	0.972(7)	0.965(5)	0.970(12)	0.950(7)
W	0.957(8)	0.974(6)	0.985(14)	0.955(9)
Ti	1.008(26)	0.957(17)	-	-

TABLE V. Photon detection efficiencies and the expected widths of ΔM peaks for χ_{c1} and χ_{c2} for the muon (first part) and the electron (second part) channels.

Mat.	$\varepsilon_{\gamma}^{\chi_{c1}}$ (%)	$\sigma_{\chi_{c1}}$ (the electron (second part) channels.)	$\varepsilon_{\gamma}^{\chi_{c2}}$ (%)	$\sigma_{\chi_{c2}}$ (MeV/ c^2)
C	40.5 ± 0.4	30.2 ± 0.4	41.2 ± 0.2	33.0 ± 0.2
W	37.1 ± 0.5	32.0 ± 0.7	38.2 ± 0.3	34.3 ± 0.5
Ti	41.3 ± 1.3	31.6 ± 0.8	41.4 ± 0.8	30.2 ± 0.3
C	39.6 ± 0.6	32.1 ± 0.4	40.4 ± 0.3	33.0 ± 0.2
W	38.6 ± 1.0	33.7 ± 0.8	38.3 ± 0.6	35.4 ± 0.4

ECAL of reconstructed electrons or positrons from photon conversions before the magnet. Since the average dilepton triggered data run contains several thousands of such reconstructible conversions, the method affords a detailed check of the stability of photon detection efficiency over the run as well as a check of the MC. The tracks from the converted photons are required to share a common silicon vertex detector track segment and to have hits in the OTR chamber immediately before the ECAL (to discriminate against electrons, which start to shower before the ECAL). When using the positron from such a pair as a probe, the electron (“tag”) is also required to have an associated ECAL cluster with a deposited energy compatible with the electron track momentum (and vice versa). For selected electron and positron probes, the ECAL is searched for a geometrically matching cluster and the ratio of the deposited ECAL energy to the track momentum (“ E/p ratio”) is entered into a histogram. Signal-to-background ratios of the order of 15 are achieved. The E/p ratio histogram of the probe as well as the corresponding E/p histogram of the tag are fitted to Gaussians to describe the signal and third order polynomials for the background description. The fit describes the data well with χ^2 values, typically equal to or less than the number of degrees of freedom. The efficiency is extracted from the fit parameters. The ratio of MC efficiencies estimates to the efficiency derived by this method is found to be 1.144 ± 0.034 , with the quoted uncertainty dominated by run-to-run variations. Roughly half the difference between efficiency estimates from MC

and data can be attributed to a higher ECAL cluster multiplicity in the data compared with the MC—when a cluster caused by a photon from a χ_c overlaps with another cluster, the photon’s measured energy becomes too large and the mass estimate incorrect. The remaining ($\approx 7\%$) discrepancy is not understood but is likely due to cases where the energy deposited by the photon (electron) is considerably less than would be expected from Gaussian statistics.

In Table V, the values of efficiency and the width of χ_{c1} and χ_{c2} are reported for the two lepton channels and for the different target materials.

VI. EVENT COUNTING

A. J/ψ counting

a. The muon channel: The $\mu^+\mu^-$ invariant mass spectra for C, Ti, and W samples as well as the summed spectrum are shown in Fig. 3 along with a fitted curve. The fit includes the J/ψ and $\psi(2S)$ peaks, each described by a superposition of three Gaussians with a common mean plus a radiative tail to describe the photon emission process $\psi \rightarrow \mu^+\mu^-\gamma$ [29], and an exponential to describe the background. The numbers of J/ψ within the mass window used for χ_c selection are reported in Table VI.

b. The electron channel: The e^+e^- invariant mass spectra for the different materials and the full sample are shown in Fig. 4. The fit used for the signals (J/ψ and $\psi(2S)$) includes a Gaussian for the right part of the peaks and, for the left part, a Breit-Wigner to take into account the

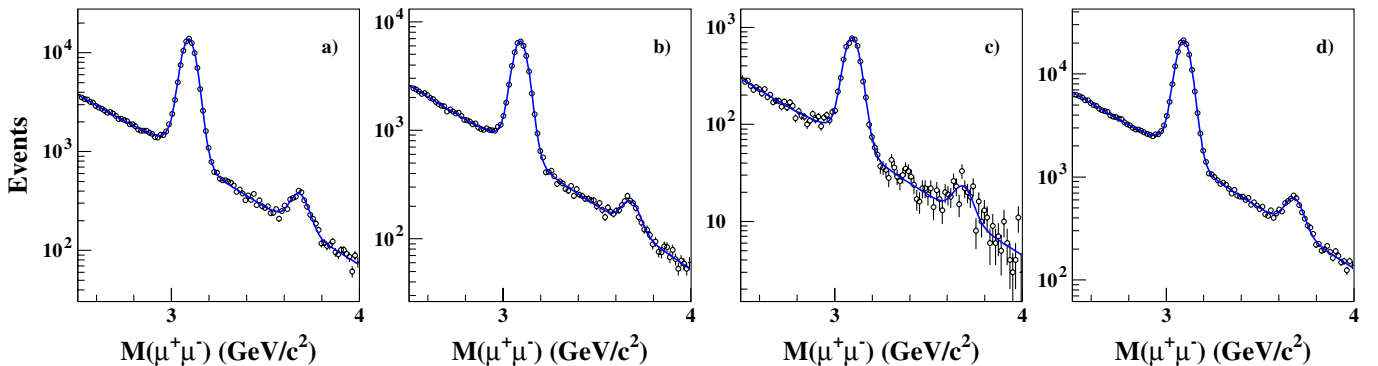


FIG. 3 (color online). $\mu^+\mu^-$ invariant mass spectra in the muon channel for C (a), W (b), Ti (c), and full sample (d). The bin width is 15 MeV/ c^2 .

TABLE VI. Total numbers of J/ψ events per target material and for the full data set in the $\mu^+\mu^-$ and e^+e^- channels.

Mat.	$\mu^+\mu^-$		e^+e^-	
	$N_{J/\psi}$	$\sigma_{J/\psi}$ (MeV/c ²)	$N_{J/\psi}$	$\sigma_{J/\psi}$ (MeV/c ²)
C	80 400 ± 300	35.6 ± 0.2	50 030 ± 530	64.2 ± 0.8
W	47 750 ± 200	36.0 ± 0.3	23 460 ± 480	66.1 ± 1.6
Ti	4 700 ± 70	37.1 ± 0.7	3 530 ± 150	58.8 ± 2.8
Tot	122 900 ± 400	35.8 ± 0.1	77 020 ± 700	64.3 ± 0.8

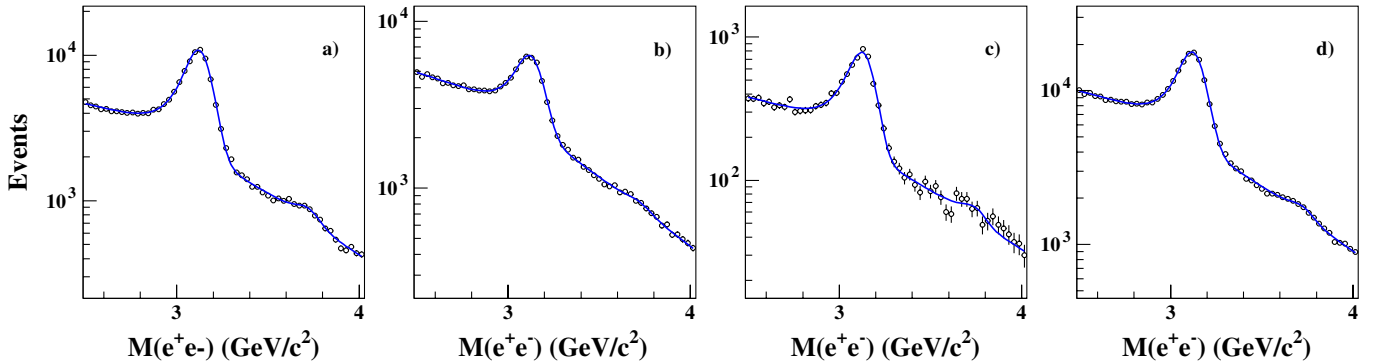
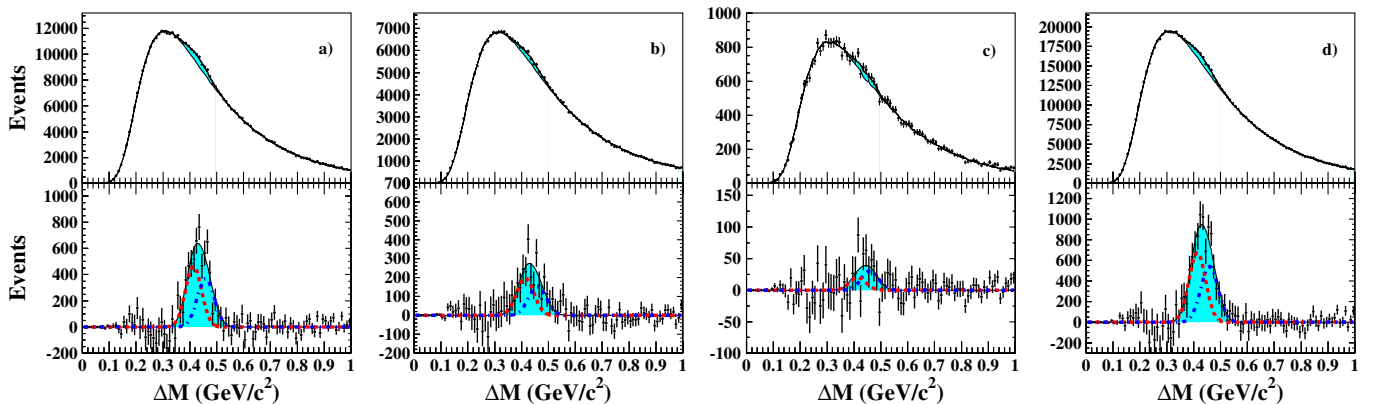
Bremsstrahlung tail, while a Gaussian (exponential) describes the background in the low (high) mass region with the requirement of continuity of the functions and of the first derivatives. The numbers of J/ψ within the mass window used for χ_c selection are reported in Table VI.

B. χ_c counting

The ΔM spectra are shown in Fig. 5 for the muon channel, and Fig. 6 for the electron channel. In the upper parts of these figures, the SE data are indicated by points. Fits to the ME and SE samples are shown as solid lines. The two curves are not distinguishable except in the ΔM

region between 0.3 and 0.6 GeV/c², where the ME curve is below the SE curve. The fit to the SE spectrum uses the ME parameterization to describe the background and Gaussian distributions for the signal, as described below. In order to evaluate the quality of the background description, the background subtracted spectra are shown below the fitted ΔM spectra for visual representation only. A clear χ_c signal is visible both in the carbon and tungsten samples, while in the titanium sample, the significance of the χ_c signal is at the level of $\sim 3.5\sigma$ only.

The detector resolution for the two χ_c states is comparable with their mass difference, resulting in a single χ_c peak in the ΔM spectrum. It is nevertheless possible to


 FIG. 4 (color online). e^+e^- invariant mass spectra for C (a), W (b), Ti (c), and full sample (d). The bin width is 30 MeV/c².

 FIG. 5 (color online). ΔM spectra in the muon channel for C (a), W (b), Ti (c), and full sample (d). The bin width is 10 MeV/c². In the background subtracted spectra the broken curves are the fitted χ_{c1} and χ_{c2} states.

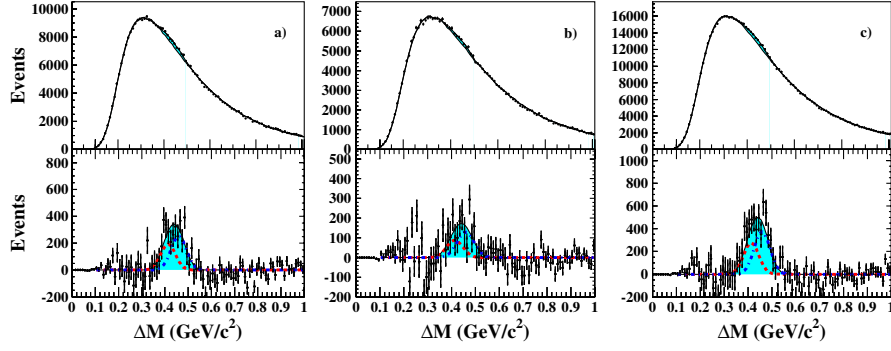


FIG. 6 (color online). ΔM spectra in the electron channel for C (a), W (b), and full sample (c). The Ti spectrum is not shown due to the low statistics. The bin width is $10 \text{ MeV}/c^2$. In the background subtracted spectra the broken curves are the fitted χ_{c1} and χ_{c2} states.

count separately the number of χ_{c1} and χ_{c2} (and therefore measure R_{12}) by using a fit with two Gaussians with some of the parameters fixed, namely,

- (1) $\Delta M_{\chi_{c1}} = 0.4137 \text{ GeV}/c^2$ [5];
- (2) $\sigma_{\chi_{c1}}$ fixed according to the MC prediction from Table V;
 $\Delta M(\chi_{c2}) - \Delta M(\chi_{c1}) = 0.0455 \text{ GeV}/c^2$ [5];
- (3) $\frac{\sigma_{\chi_{c2}}}{\sigma_{\chi_{c1}}} = 1.05$ as predicted by MC.

The free parameters are $N_{\chi_c} = N_{\chi_{c1} + \chi_{c2}}$, $\frac{N_{\chi_{c1}}}{N_{\chi_{c2}}}$ and the ME normalization parameter. In Table VII, the values of the fitted N_{χ_c} and $\frac{N_{\chi_{c1}}}{N_{\chi_{c2}}}$ are reported for both the electron and muon channels together with the χ_c counting obtained with a single-Gaussian fit, where the χ_c is considered as a single peak.

In order to verify the assumptions made, a systematic study of the effect of releasing the different fixed parameters or varying them within a range around the assumed values was done, as well as a cross check of the χ_c counting with the signal modeled as a single Gaussian to describe both χ_c states. The results of these studies are discussed in Sec. VIII.

VII. POLARIZATION

The experimental determination of polarization can be used to probe assumptions on the impact of specific QCD processes and the influence of nuclear effects. The data available for this analysis of χ_c production does not allow a determination of the polarization of the χ_c states because of large backgrounds. In the following, we discuss angular distributions for the decay products of χ_c and directly produced J/ψ states with the goal of investigating the possible influences of polarization on the acceptances and thus on the determination of the χ_c rates. For those models that predict the polarization of states, we supply information to correct the R_{χ_c} measurements that assume no polarization.

A. χ_c polarization

The full angular distribution of final state particles in the radiative decay

$$\chi_{cJ} \rightarrow \gamma J/\psi \rightarrow \gamma l^+ l^- \quad (6)$$

can be found for pure χ_c polarization states $|J, M\rangle$ with $J = 1, 2$, and $|M| = 0, \dots, J$ in the appendix. The angular distribution formulae are independent of the choice

TABLE VII. Results of the fit of the χ_c signal in the $\mu^+ \mu^-$ and $e^+ e^-$ channels. See text for the meaning of the different fit procedures.

Mat.	1-G fit		2-G fit	
	N_{χ_c}	$N_{\chi_{c1} + \chi_{c2}}$	$\frac{N_{\chi_{c1}}}{N_{\chi_{c2}}}$	$\sigma(\chi_{c1})$
	$\mu^+ \mu^-$			
C	6280 ± 510	6390 ± 420	1.20 ± 0.26	0.030
W	3120 ± 560	2830 ± 330	1.26 ± 0.52	0.032
Ti	390 ± 110	390 ± 110	0.63 ± 0.63	0.030
Tot	9570 ± 710	9630 ± 550	1.19 ± 0.24	0.031
	$e^+ e^-$			
	N_{χ_c}	$N_{\chi_{c1} + \chi_{c2}}$	$\frac{N_{\chi_{c1}}}{N_{\chi_{c2}}}$	$\sigma(\chi_{c1}) \text{ (GeV}/c^2)$
C	3890 ± 480	3600 ± 390	0.79 ± 0.31	0.032
W	2080 ± 370	1870 ± 330	0.71 ± 0.48	0.034
Tot	5630 ± 660	5250 ± 500	0.76 ± 0.28	0.033

of a particular polarization axis (e.g. Gottfried-Jackson, Collins-Soper or other systems can be used). Possible coherent mixtures are not considered here, because we assume that a study of the pure states will be sufficient to determine systematic acceptance effects due to polarization.

If one assumes no azimuthal dependence for the production process, the χ_c decay depends on three angles which are chosen as follows: a polar decay angle θ defining the direction of the J/ψ in the χ_c rest system with respect to the polarization direction; a polar angle, θ' , defining the direction of the positive lepton in the J/ψ rest system with respect to the J/ψ direction (in the χ_c rest system); an azimuth angle, ϕ' , which is the angle between the plane defined by the polarization axis and the J/ψ direction, and the decay plane of the J/ψ .

For a state $|J, M\rangle$ the angular distribution can be decomposed into terms with trigonometric expressions $T_i^J(\theta, \theta', \phi')$ and coefficients $K_i^{J,M}$ [43]

$$W^{J,M}(\theta, \theta', \phi') = \sum_i K_i^{J,M} T_i^J(\theta, \theta', \phi'). \quad (7)$$

The angular functions $T_i^J(\theta, \theta', \phi')$ and the coefficients $K_i^{J,M}$, expressed in terms of helicity amplitudes, are reported in Table X in the appendix. With the additional assumption that for both χ_c states only the leading multipole, the electric dipole, contributes to the radiative decay, the coefficients $K_i^{J,M}$ are uniquely defined (see appendix for the numerical values). The assumption that higher order multipoles can be neglected is well justified by experimental results [5]. The pure χ_c polarization states are thus unambiguously defined.

B. J/ψ polarization

1. J/ψ angular distributions

In leptonic J/ψ decays, the J/ψ polarization can be determined from the angular distribution of the leptons. After integrating over the azimuthal orientation of the decay plane of the J/ψ (or assuming azimuthal symmetry) the distribution of the polar decay angle θ' can be parameterized as

$$\frac{1}{N} \frac{dN}{d \cos \theta'} = a(\lambda)(1 + \lambda \cos^2 \theta'),$$

$$a(\lambda) = \frac{1}{2(1 + \lambda/3)}, \quad (8)$$

where θ' is the angle between the l^+ and the quantization axis. The form of the distribution (8) is independent of the chosen quantization axis (in general however the value of λ is dependent on this choice).

2. J/ψ polarization measurement

A measurement of J/ψ polarization by the HERA-B collaboration is reported in [44]. However, the J/ψ sample

used for this study includes not only directly produced J/ψ but also J/ψ from χ_c , and it is not possible to distinguish between the two contributions. Therefore, the λ value derived from the observed distribution λ_{obs} has to be considered as the average J/ψ polarization parameter, independent of the origin.

The polarization parameters have been determined using as quantization axis, the bisector of the angle between \mathbf{p}_b and \mathbf{p}_t , where \mathbf{p}_b , \mathbf{p}_t are the momenta of the beam proton and the target nucleon, respectively, in the J/ψ center-of-mass system (“Collins-Soper frame”). The experimental value of the polarization parameter, averaged over the muon and the electron decay channels and on the target materials, and assuming no dependence on $p_T^{J/\psi}$ and $x_F^{J/\psi}$ in the HERA-B acceptance, is [44]

$$\lambda_{\text{obs}} = -0.35 \pm 0.04. \quad (9)$$

C. Method for the evaluation of systematic uncertainties due to polarization

In this section, we explain the method used to estimate the systematic uncertainties for R_{χ_c} and R_{12} arising from possible polarizations of the χ_c and directly produced J/ψ states. The only experimental constraint that can be used for these estimations is the measured λ_{obs} (Sec. VII B 2).

1. Principle of the method

The efficiencies entering in the formulae for R_{χ_c} and R_{12} (3) and (4) depend in general on the polarization of the χ_c and the directly produced J/ψ states. The efficiencies will be evaluated for the χ_c pure polarization states described in Sec. VII A, which will then be used to limit the ranges of possible R_{χ_c} and R_{12} values and will in turn be used to determine the uncertainties of these values in Sec. VIII B. As in the J/ψ analysis [44], we evaluate the polarization states in the Collins-Soper frame. Despite this specific choice and the restriction to pure polarization states, we expect to obtain a representative estimate of uncertainties induced by polarization.

The formulae for R_{χ_c} and R_{12} require the detection efficiency for direct J/ψ production $\varepsilon_{J/\psi}^{\text{dir}}$, which depends on the polarization parameter λ_{dir} . Since the observed polarization λ_{obs} also includes the effect of possible χ_c polarization, λ_{dir} has to be disentangled from it using the values λ_1 and λ_2 obtained for the assumed polarization states of χ_{c1} and χ_{c2} , respectively. This is done with an iterative procedure in which the yet-to-be-determined values of R_{χ_c} and R_{12} are used as inputs.

2. Determination of λ_{dir} , λ_1 , λ_2

Starting from Eq. (8), the observed polar decay angle distribution can be decomposed into contributions from directly produced J/ψ and J/ψ from χ_{c1} and χ_{c2} events

$$a_{\text{obs}}(1 + \lambda_{\text{obs}} \cos^2 \theta') = \sum_{i=\text{dir},1,2} f_i a_i (1 + \lambda_i \cos^2 \theta'), \quad (10)$$

with $a_i = a(\lambda_i)$. The fractions f_i ($i = \text{dir}, 1, 2$) of the different types of J/ψ are determined by R_{χ_c} and R_{12} . With $\sum_i f_i = 1$, $f_1 + f_2 = R_{\chi_c}$, and $f_1/f_2 = R_{12}$ one obtains

$$f_{\text{dir}} = 1 - R_{\chi_c}, \quad f_1 = \frac{R_{\chi_c} R_{12}}{1 + R_{12}}, \quad f_2 = \frac{R_{\chi_c}}{1 + R_{12}}. \quad (11)$$

Since there is no direct measurement of λ_1 and λ_2 , the angular distributions corresponding to the different pure polarization states $|J, M\rangle$ of χ_{c1} and χ_{c2} described in Sec. VII A are used to determine the subranges allowed for λ_1 and λ_2 , out of the full $[-1.0, 1.0]$ interval. For this purpose, the unpolarized χ_c angular distribution is re-weighted with the corresponding function (7). The resulting $\cos\theta'$ distribution is then fitted with the function (8), which then yields λ_1 or λ_2 corresponding to the tested pure χ_c polarization state.

Solving (10) for λ_{dir} as a function of λ_{obs} for given values of λ_1 , λ_2 , R_{χ_c} , and R_{12} yields

$$\lambda_{\text{dir}}(\lambda_{\text{obs}} | \lambda_1, \lambda_2, R_{\chi_c}, R_{12}) = \frac{a_{\text{obs}} \lambda_{\text{obs}} - a_1 f_1 \lambda_1 - a_2 f_2 \lambda_2}{a_{\text{obs}} - a_1 f_1 - a_2 f_2}. \quad (12)$$

In this equation, R_{χ_c} and R_{12} enter via the fractions f_i . On the other hand, as both depend also on λ_{dir} , an iterative procedure is applied starting with $\lambda_{\text{dir}} = 0$.

3. Polarization dependence of the efficiencies

For each tested pure χ_c polarization state with the corresponding set of values λ_{dir} , λ_1 , λ_2 , new efficiencies ε_γ and $\varepsilon_{J/\psi}$ are determined.

a. J/ψ efficiencies: Assuming no dependence of λ on $x_F^{J/\psi}$ and $p_T^{J/\psi}$ (approximately valid within the uncertainty of our measurement [44]), we can write $\varepsilon_{J/\psi}(\lambda)$ as

$$\begin{aligned} \varepsilon_{J/\psi}(\lambda) &= \frac{N_{\text{reco}}^{J/\psi}}{N_{\text{gen}}^{J/\psi}} \\ &= \frac{\int A(\cos\theta', P) \cdot M(P) \cdot (1 + \lambda \cos^2 \theta') \cdot d\cos\theta' dP}{\int M(P) \cdot (1 + \lambda \cos^2 \theta') \cdot d\cos\theta' dP}, \end{aligned} \quad (13)$$

where θ' is the polar angle in the polarization frame, P is shorthand for all the other phase space variables, $A(\cos\theta', P)$ is the acceptance at the kinematical point $(\cos\theta', P)$, $M(P)$ is the squared matrix element in P , and λ is the polarization parameter. After calculating the integrals we find

$$\varepsilon_{J/\psi}(\lambda) = \varepsilon_{J/\psi}(\lambda = 0) \frac{1 + \lambda \cdot \langle \cos^2 \theta' \rangle}{(1 + \lambda/3)}, \quad (14)$$

where $\langle \cos^2 \theta' \rangle$ is given by

$$\langle \cos^2 \theta' \rangle = \frac{\int A(\cos\theta', P) \cdot M(P) \cdot \cos^2 \theta' \cdot d\cos\theta' dP}{\int A(\cos\theta', P) \cdot M(P) \cdot d\cos\theta' dP}.$$

All J/ψ efficiencies, both for direct J/ψ and for J/ψ from the two χ_c states, are calculated using Eq. (14).

b. Photon efficiencies: To determine the effect of polarization on the photon efficiencies, we start with the formula

$$\varepsilon_\gamma^{\chi_{cJ}} = \frac{N_{\chi_{cJ,M}}}{N_{J/\psi}^{\chi_{cJ,M}}}, \quad (15)$$

where J, M denotes the polarization state considered, $N_{J/\psi}^{\chi_{cJ,M}}$ is the number of J/ψ coming from χ_{cJ} , and $N_{\chi_{cJ,M}}$ is the number of observed χ_{cJ} . The value of $N_{J/\psi}^{\chi_{cJ,M}}$ is obtained from a fit of the $l^+ l^-$ mass distribution, where each event enters with a weight

$$w(\cos\theta', \lambda_{J,M}) = \frac{1 + \lambda_{J,M} \cdot \cos^2 \theta'}{(1 + \lambda_{J,M}/3)}. \quad (16)$$

The value of $N_{\chi_{cJ,M}}$ is obtained from a fit of the ΔM distribution of true χ_{cJ} (using MC generator information to select the correct $J/\psi\gamma$ combination), where the weight for each entry in the histogram corresponds to a certain pure polarization state of χ_{cJ} , calculated by Eq. (7).

VIII. SYSTEMATIC UNCERTAINTIES

A. Uncertainties from reconstruction, calibration, simulation, and background subtraction

With the exception of J/ψ counting, all of the systematic uncertainties in the measurement of R_{χ_c} are common to the e^+e^- and $\mu^+\mu^-$ channels, as the use of the mass difference distribution almost completely removes the uncertainty due to the lepton selection and measurement. The overall uncertainty is therefore completely dominated by the photon selection in the calorimeter, which is common to the two lepton channels. The J/ψ counting systematic uncertainties are estimated to be 2% in the electron channel and 0.25% in the muon channel. The remaining systematic uncertainty estimates include

χ_c counting:

- (1) photon selection (7%);
- (2) variation of $l^+ l^-$ mass window (2%);
- (3) χ_c signal fitting procedure (4%) including:
 - (a) variation of the fixed parameters of the double-Gaussian fit: $\Delta M_{\chi_{c1}}$, $\sigma_{\chi_{c1}}$, $\Delta M(\chi_{c2}) - \Delta M(\chi_{c1})$, and $\frac{\sigma_{\chi_{c2}}}{\sigma_{\chi_{c1}}}$;
 - (b) fit with free $\Delta M_{\chi_{c1}}$ and/or $\sigma_{\chi_{c1}}$;
 - (c) change of binning of the ΔM spectrum.

- (4) Extensive tests were performed on the background determination with the mixed event procedure:
 - (a) Variation of corrections corresponding to combinations of J/ψ 's with photons from χ_c decays in ME, which do not occur in SE (+3%);
 - (b) Relaxing the requirement of the same neutral cluster multiplicity in ME and SE ($\pm 2\%$);
 - (c) Variation of the cut on the neutral cluster direction in ME with respect to SE ($\pm 3\%$);
 - (d) Allowing for an additional, polynomial term in the background to improve the fit around the χ_c signal yields an asymmetric uncertainty (+4%).

The total contribution from the background description to the systematic uncertainty in the χ_c counting is estimated to range between -4% and $+6\%$.

Efficiency evaluation

- (a) The use of different kinematic distributions for the generation of the J/ψ (see Refs. [29,38]), affecting both $\frac{\varepsilon_{J/\psi}^{\chi_c}}{\varepsilon_{dir}^{J/\psi}}$ and ε_γ , introduces a systematic effect on R_{χ_c} of 4%;
- (b) Tests on the photon efficiency simulation were performed including the comparison between real data and Monte Carlo of the γ conversion yield and of the detection efficiency of photons from electron Bremsstrahlung. The overall systematic uncertainty on ε_γ determination and correction is found to be 6.5%.

The overall systematic uncertainty on R_{χ_c} , evaluated as the quadratic sum of the above terms, is therefore $^{+13}_{-12}\%$ for both J/ψ decay channels.

The systematic uncertainty on R_{12} is completely dominated by the accuracy of the ECAL energy calibration, which affects both $\Delta M(\chi_{c1})$ and its resolution, the first affecting in turn the ratio $\frac{N_{\chi_{c1}}}{N_{\chi_{c2}}}$. A fine-tuning of the ECAL calibration as a function of the photon energy was performed using the $\pi^0 \rightarrow \gamma\gamma$ signal. An absolute calibration accuracy of $\sim 2\%$ was obtained and on $\Delta M_{\chi_{c1}}$ of $\sim 8 \text{ MeV}/c^2$. By scanning $\Delta M(\chi_{c1})$ in such range around the nominal value [5], a variation of $\frac{N_{\chi_{c1}}}{N_{\chi_{c2}}}$ (and thus R_{12}) of 35% is obtained. No effect on R_{12} is observed by changing the other fixed fit parameters.

B. Polarization effects

Since the direct J/ψ and χ_c polarizations cannot be determined separately from our data, we estimate instead systematic uncertainties on the reference values reported in Table VIII (and denoted by $R_{\chi_c}^{\text{ref}}$ and R_{12}^{ref} in the following), which were obtained with the assumption of zero polarization. The results of this study are expressed as overall shifts of the values of R_{χ_c} and R_{12} due to the average polarization of directly produced J/ψ with uncertainties obtained from the maximum variation of χ_c polarizations allowed by the

measurement

$$\frac{R_{\chi_c} - R_{\chi_c}^{\text{ref}}}{R_{\chi_c}^{\text{ref}}} = +9.5\%_{-7\%}^{+11\%} \quad \frac{R_{12} - R_{12}^{\text{ref}}}{R_{12}^{\text{ref}}} = +0\%_{-11\%}^{+16\%}, \quad (17)$$

where the following ingredients are used:

- (1) The central values are obtained from the average measured value for λ_{obs} and with the assumption of no polarization of χ_{c1} and χ_{c2} ($\lambda_{\text{obs}} = -0.35$, $\lambda_1 = 0$, and $\lambda_2 = 0$, yielding $\lambda_{\text{dir}} = -0.424$). Therefore, if the observed J/ψ polarization were due exclusively to direct J/ψ polarization, the measured R_{χ_c} would be shifted up by 9.5%, while obviously no effect on R_{12} is produced.
- (2) The variation bands in Eq. (17) are obtained by taking the extreme positive and negative variations of the central values defined above, of all combinations of λ_{obs} [varied in a 95% c.l. range around the measured value, see Eq. (9)] with λ_1 and λ_2 (corresponding to the different pure helicity states M1 and M2):
 - (a) upper value: $\lambda_{\text{obs}} = -0.44$; $\lambda_1 = -0.24$, $\lambda_2 = 0.18$ for R_{χ_c} ; $\lambda_1 = -0.24$, $\lambda_2 = -0.18$ for R_{12} ;
 - (b) lower value: $\lambda_{\text{obs}} = -0.26$; $\lambda_1 = 0.22$ and $\lambda_2 = -0.18$ for R_{χ_c} ; $\lambda_1 = 0.22$ and $\lambda_2 = 0.18$ for R_{12} .
- (3) Different polarization values give overlapping ranges of possible R_{χ_c} and R_{12} values. Any value in each range is equally probable. Thus, even if the error on λ_{obs} were Gaussian distributed, the errors of R_{χ_c} and R_{12} would not be Gaussian distributed. To take into account that the polarization parameter λ_{obs} was determined as an average over the whole accepted phase space and over different materials, λ_{obs} was varied in a $\pm 2\sigma$ range with equal weights. Selecting the maximum deviations the measured values R_{χ_c} and R_{12} would have to be scaled:

$$R_{\chi_c} = f_{R_{\chi_c}} \cdot R_{\chi_c}^{\text{ref}} \quad R_{12} = f_{R_{12}} \cdot R_{12}^{\text{ref}}, \quad (18)$$

with $f_{R_{\chi_c}} \in [1.02, 1.21]$ and $f_{R_{12}} \in [0.89, 1.16]$, where the uncertainties due to polarization are fully contained in the ranges given.

- (4) Note that the correlation between the values of R_{χ_c} and R_{12} are ignored in Eqs. (17) and (18).

IX. RESULTS

A. R_{χ_c}

The measured values for R_{χ_c} are computed from Eq. (3), assuming zero J/ψ polarization and are reported in Table VIII, separately for muon and electron channels and combined sample. When averaged over decay channels and target materials, a value of

$$R_{\chi_c} = 0.188 \pm 0.013_{\text{st}} \begin{matrix} +0.024 \\ -0.022_{\text{sys}} \end{matrix} \quad (19)$$

is obtained. The quoted uncertainties include all systematic contributions (except the polarization contribution, which is given in Eq. (17) as a variation band at 95% c.l.). The following observations can be made:

- (1) The results obtained in the two lepton channels are compatible within 1σ in both C and W samples. No measurement for the Ti in the electron channel is possible due to the low statistics;
- (2) The values of R_{χ_c} obtained separately in the three target samples are consistent with each other;
- (3) The present result is lower than most values published in the literature in pN interactions (see Table III and Fig. 1). Despite the fact that the various available measurements are taken at widely differing center of mass energies, they are for the most part compatible within $\sim 1.5\sigma$, except for E705 (2.3σ) and R806 (3.3σ). The present measurement is lower than the previous HERA-B result [15] by about 2σ . The two analyses are quite similar, although more extensive systematic checks have been performed in connection with the present one. These checks did not uncover any error in the previous analysis, and we thus believe that the differences are largely statistical. The average of the two HERA-B results, $R_{\chi_c} = 0.198^{+0.028}_{-0.026}$, differs by less than 1σ from the result of Eq. (19).

B. R_{12}

The measured values of R_{12} are evaluated using Eq. (4), assuming no polarization for either the directly produced J/ψ 's or the χ_c 's, and are summarized in Table VIII.

As above, no dependence on target material is observed. The results from the electron channel are consistently lower than the muon results, but nonetheless in agreement to within 1σ of the statistical uncertainties.

The final result averaged over decay channel and target material is

$$R_{12} = 1.02 \pm 0.17_{\text{st}} \pm 0.36_{\text{sys}}, \quad (20)$$

where the systematic uncertainty does not include the polarization contribution, which is given in Eq. (17) as a variation band at 95% c.l. The J/ψ yields from χ_{c1} and χ_{c2} are therefore found to be equal, although with large uncertainties.

C. Dependence on kinematic variables

A study of the dependence of R_{χ_c} on the kinematic variables $x_F^{J/\psi}$ and $p_T^{J/\psi}$ in the ranges covered by HERA-B ($x_F^{J/\psi} \in [-0.35, 0.15]$, $p_T^{J/\psi} \lesssim 5 \text{ GeV}/c$) was performed by applying the described procedure in five $x_F^{J/\psi}$ and three $p_T^{J/\psi}$ intervals, respectively. The resulting distributions, for both channels combined, are shown in Fig. 7(a) and 7(b). The data is compatible with a flat dependence of R_{χ_c} on both kinematic variables, although more complex dependences cannot be ruled out.

D. A-dependence

The atomic mass number (A) dependence of inclusive cross sections is often parameterized as a power law

$$\sigma_{\text{pA}} = \sigma_{\text{pN}} A^\alpha, \quad (21)$$

where σ_{pA} is the inclusive production cross section in

TABLE VIII. Measured values of R_{χ_c} , R_{12} and $\frac{\sigma(\chi_{c1})}{\sigma(\chi_{c2})}$ in e^+e^- , $\mu^+\mu^-$ and combined sample for the different materials and the full data sample.

Mat.	e^+e^-	$\mu^+\mu^-$	combined
R_{χ_c}			
C	$0.174 \pm 0.029_{\text{st}} \begin{matrix} +0.022 \\ -0.021_{\text{sys}} \end{matrix}$	$0.190 \pm 0.018_{\text{st}} \begin{matrix} +0.024 \\ -0.022_{\text{sys}} \end{matrix}$	$0.185 \pm 0.015_{\text{st}} \begin{matrix} +0.024 \\ -0.022_{\text{sys}} \end{matrix}$
Ti	–	$0.197 \pm 0.079_{\text{st}} \begin{matrix} +0.025 \\ -0.023_{\text{sys}} \end{matrix}$	$0.197 \pm 0.079_{\text{st}} \begin{matrix} +0.025 \\ -0.023_{\text{sys}} \end{matrix}$
W	$0.202 \pm 0.055_{\text{st}} \begin{matrix} +0.026 \\ -0.024_{\text{sys}} \end{matrix}$	$0.191 \pm 0.034_{\text{st}} \begin{matrix} +0.025 \\ -0.022_{\text{sys}} \end{matrix}$	$0.194 \pm 0.029_{\text{st}} \begin{matrix} +0.025 \\ -0.023_{\text{sys}} \end{matrix}$
Tot	$0.180 \pm 0.025_{\text{st}} \begin{matrix} +0.023 \\ -0.021_{\text{sys}} \end{matrix}$	$0.190 \pm 0.015_{\text{st}} \begin{matrix} +0.024 \\ -0.022_{\text{sys}} \end{matrix}$	$0.188 \pm 0.013_{\text{st}} \begin{matrix} +0.024 \\ -0.022_{\text{sys}} \end{matrix}$
R_{12}			
C	$0.82 \pm 0.32_{\text{st}}$	$1.23 \pm 0.27_{\text{st}}$	$1.06 \pm 0.21_{\text{st}} \pm 0.37_{\text{sys}}$
Ti	–	$0.67 \pm 0.67_{\text{st}}$	$0.67 \pm 0.67_{\text{st}} \pm 0.23_{\text{sys}}$
W	$0.73 \pm 0.49_{\text{st}}$	$1.27 \pm 0.53_{\text{st}}$	$0.98 \pm 0.36_{\text{st}} \pm 0.34_{\text{sys}}$
Tot	$0.79 \pm 0.27_{\text{st}}$	$1.17 \pm 0.22_{\text{st}}$	$1.02 \pm 0.17_{\text{st}} \pm 0.36_{\text{sys}}$
$\frac{\sigma(\chi_{c1})}{\sigma(\chi_{c2})}$			
C	$0.47 \pm 0.19_{\text{st}}$	$0.70 \pm 0.16_{\text{st}}$	$0.60 \pm 0.12_{\text{st}} \pm 0.21_{\text{sys}}$
Ti	–	$0.38 \pm 0.38_{\text{st}}$	$0.38 \pm 0.38_{\text{st}} \pm 0.13_{\text{sys}}$
W	$0.41 \pm 0.28_{\text{st}}$	$0.72 \pm 0.30_{\text{st}}$	$0.56 \pm 0.21_{\text{st}} \pm 0.20_{\text{sys}}$
Tot	$0.45 \pm 0.16_{\text{st}}$	$0.66 \pm 0.13_{\text{st}}$	$0.57 \pm 0.10_{\text{st}} \pm 0.20_{\text{sys}}$

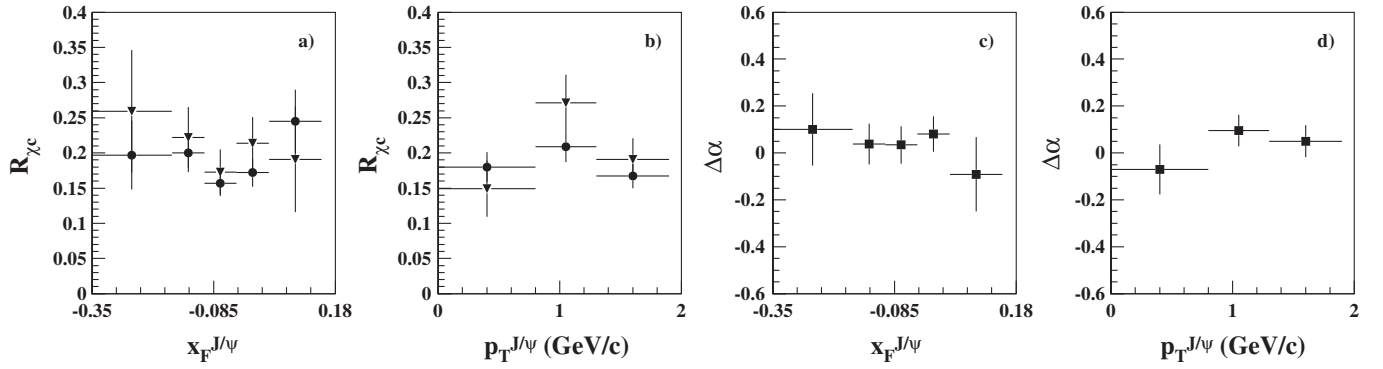


FIG. 7. Dependence of R_{χ_c} on $x_F^{J/\psi}$ (a) and $p_T^{J/\psi}$ (b) [circles: C; triangles: W]. Dependence of $\Delta\alpha = \alpha_{\chi_c} - \alpha_{J/\psi}$ on $x_F^{J/\psi}$ (c) and $p_T^{J/\psi}$ (d). Only statistical errors are shown.

collisions of protons with a nuclear target of atomic mass number A , σ_{pN} is the average cross section in collisions of protons with a single nucleon and α characterizes the A -dependence of the cross section. The difference between α for J/ψ production and that for χ_c production can be computed from the measured values of R_{χ_c} for C and W targets given in Table VIII from the following formula:

$$\Delta\alpha = \alpha_{\chi_c} - \alpha_{J/\psi} = \frac{1}{\log \frac{A_W}{A_C}} \cdot \log \frac{R_{\chi_c}^W}{R_{\chi_c}^C}, \quad (22)$$

where $A_W = 184$ and $A_C = 12$ are the tungsten and carbon atomic mass numbers. The results, plotted as a function of $x_F^{J/\psi}$ and $p_T^{J/\psi}$ are shown in Figs. 7(c) and 7(d). Averaged over the visible $x_F^{J/\psi}$ and $p_T^{J/\psi}$ range, $\Delta\alpha = 0.05 \pm 0.04$. The predictions of the various production models for $\Delta\alpha$ are all within the uncertainties of the measurement [6].

E. χ_c cross sections and ratio

From Eq. (5) we obtain the values for the cross section ratio $\frac{\sigma(\chi_{c1})}{\sigma(\chi_{c2})}$ under the assumption of zero polarization for both J/ψ and χ_c . The results are reported in Table VIII. The target material averaged result is

$$\frac{\sigma(\chi_{c1})}{\sigma(\chi_{c2})} = 0.57 \pm 0.23, \quad (23)$$

where the uncertainty includes the systematic contributions (except polarization—see above). The χ_c production cross sections, defined as

$$\sigma(\chi_{ci}) = \frac{\sigma(J/\psi)R_{\chi_{ci}}}{\text{Br}(\chi_{ci} \rightarrow J/\psi\gamma)}, \quad i = 1, 2 \quad (24)$$

are calculated using the estimate of the total J/ψ cross section at $\sqrt{s} = 41.6$ GeV, $\sigma(J/\psi) = (502 \pm 44)$ nb/nucleon reported in [30] and assuming that R_{χ_c} is independent of $x_F^{J/\psi}$ over the full $x_F^{J/\psi}$ and $p_T^{J/\psi}$ range. The

following target material averaged values are obtained:

$$\begin{aligned} \sigma(\chi_{c1}) &= 133 \pm 35 \text{ nb/nucleon}; \\ \sigma(\chi_{c2}) &= 231 \pm 61 \text{ nb/nucleon}, \end{aligned} \quad (25)$$

leading to a total χ_c production cross section $\sigma(\chi_c) = 364 \pm 74$ nb/nucleon. Figure 1 shows all available measurements of the χ_{c1} and χ_{c2} production cross sections and their ratio in proton-nucleus interactions at fixed-target energies.

X. CONCLUSION

We have presented a new measurement of the fraction of all J/ψ mesons produced through χ_c decay (R_{χ_c}), performed with the HERA-B detector in pC , pTi , and pW interactions at 920 GeV/c ($\sqrt{s} = 41.6$ GeV). The χ_c mesons were detected in the $J/\psi\gamma$ decay mode, and the J/ψ in both $\mu^+\mu^-$ and e^+e^- decay modes. The detector acceptance was flat in $p_T^{J/\psi}$ and extended from $x_F^{J/\psi} = -0.35$ to $x_F^{J/\psi} = 0.15$.

The measurement is based on a total sample of ~ 15000 χ_c , the largest ever observed in pA collisions. Apart from lepton identification requirements, the analysis is identical for the two channels. The separate results for the two channels are found to be in agreement with each other in all respects.

The measured value $R_{\chi_c} = 0.188 \pm 0.013_{\text{st}-0.022_{\text{sys}}}$ is $\sim 2\sigma$ lower than the previously published result from HERA-B. Our new value is also lower than, but not incompatible with, most of the previously published values obtained from pN interactions, independent of the center of mass energies and the kinematic ranges of the measurements. The present result supports the NRQCD calculations [6]. When taken together with the already published result of HERA-B on $\psi(2S)$ production [29], the fraction of all J/ψ mesons coming from decays of higher mass charmonium states is found to be $\sim 27\%$.

By separately counting the contribution of χ_{c1} and χ_{c2} , we obtain a ratio of the two states $R_{12} = R_{\chi_{c1}}/R_{\chi_{c2}} = 1.02 \pm 0.40$ and a cross section ratio $\frac{\sigma(\chi_{c1})}{\sigma(\chi_{c2})} = 0.57 \pm 0.23$. The χ_{c1} and χ_{c2} cross sections are measured to be $\sigma(\chi_{c1}) = 133 \pm 35$ nb/nucleon and $\sigma(\chi_{c2}) = 231 \pm 61$ nb/nucleon in the full $x_F^{J/\psi}$ range.

No significant departure from a flat dependence of R_{χ_c} on the kinematic variables $x_F^{J/\psi}$ and $p_T^{J/\psi}$ is found within the limited accuracy of our measurement. No significant difference in the A-dependence of χ_c and J/ψ production is found within the limits of the available statistics.

For the first time, an evaluation of the effect of polarization of J/ψ and χ_c on the measured values of R_{χ_c} and R_{12} was performed. The behavior of R_{χ_c} and R_{12} as a function of the polarization, expressed by the λ parameter, was studied with the conclusion that R_{χ_c} and R_{12} are uncertain with factors in the ranges [1.02,1.21] and [0.89,1.16], respectively, ignoring correlations between the two.

No mention of the influence of polarization on the measurement of R_{χ_c} can be found in any of the previous measurements. Nonetheless, we suspect that all measurements are subject to similar uncertainties to greater or lesser extents, depending on the geometry of the apparatus used.

ACKNOWLEDGMENTS

We express our gratitude to the DESY laboratory for the strong support in setting up and running the HERA-B experiment. We are also indebted to the DESY accelerator group for its continuous efforts to provide good and stable beam conditions. The HERA-B experiment would not have been possible without the enormous effort and commitment of our technical and administrative staff. It is a pleasure to thank all of them. We acknowledge support from the Foundation for Fundamental Research on Matter (FOM), 3502 GA Utrecht, The Netherlands; CICYT under Contract No. AEN99-0483; the German Research Foundation, Graduate College under Contract No. GRK 271/3; the Bundesministerium für Bildung und Forschung, FRG, under Contract Nos. 05-7BU35I, 05-7DO55P, 05-HB1HRA, 05-HB1KHA, 05-HB1PEA, 05-HB1PSA, 05-HB1VHA, 05-HB9HRA, 05-7HD15I, 05-7MP25I, 05-7SI75, the Portuguese Fundação para a Ciência e Tecnologia under the POCTI program; the Danish Natural Science Research Council; the National Academy of Science and the Ministry of Education and Science of Ukraine; the Ministry of Education, Science, and Sport of the Republic of Slovenia under Contract Nos. P1-135 and J1-6584-0106; the U.S. National Science Foundation under Grant No. PHY-9986703; the Russian Ministry of Education and Science under Grant No. SS-1722.2003.2; the BMBF; the Norwegian Research Council; and the Swiss National Science Foundation.

APPENDIX: χ_c ANGULAR DISTRIBUTIONS

The angular decay distribution of a pure polarization state $|J, M\rangle$ is given as an expansion into helicity amplitudes $A_{|\nu|}^J$ by [43]

$$W^{J,M}(\theta, \theta', \phi') = \sum_{\nu, \nu' = -J}^{+J} \sum_{\mu = \pm 1} d_{M\nu}^J(\theta) d_{M\nu'}^{J*} \times (\theta) A_{|\nu|}^J \rho^{\sigma\sigma'}(\theta', \phi'), \quad (\text{A1})$$

with the density matrix for the J/ψ helicity (Table IX)

$$\rho^{\sigma\sigma'}(\theta', \phi') = \sum_{\kappa = \pm 1} D_{\sigma\kappa}^1(\phi', \theta', -\phi') D_{\sigma'\kappa}^{1*}(\phi', \theta', -\phi'). \quad (\text{A2})$$

Using the notation of [43] the angular distribution can be decomposed into terms with trigonometric expressions $T_i^J(\theta, \theta', \phi')$ and coefficients $K_i^{J,M}(A_{|\nu|}^J)$

$$W^{J,M}(\theta, \theta', \phi') = \sum_i K_i^{J,M}(A_{|\nu|}^J) T_i^J(\theta, \theta', \phi'). \quad (\text{A3})$$

The $K_i^{J,M}(A_{|\nu|}^J)$ and $T_i^J(\theta, \theta', \phi')$ are reported for $J = 1, 2$ in Table X. The normalizations are for the angular distributions

$$\int W^{J,M}(\theta, \theta', \phi') d \cos\theta d\phi d \cos\theta' d\phi' = \begin{cases} \frac{64\pi^2}{9} & \text{for } J = 1 \\ \frac{64\pi^2}{15} & \text{for } J = 2. \end{cases} \quad (\text{A4})$$

The helicity amplitudes $A_{|\nu|}^J$ can be expanded in multipole amplitudes (E1, M2, E3), see for example [43]. With the restriction to electric dipole transitions the helicity amplitudes become

$$J = 1: A_0 = \sqrt{\frac{1}{2}}, \quad A_1 = \sqrt{\frac{1}{2}} \quad J = 2: A_0 = \sqrt{\frac{1}{10}}, \\ A_1 = \sqrt{\frac{3}{10}} \quad A_2 = \sqrt{\frac{3}{5}}. \quad (\text{A5})$$

Table X reports also the coefficients $K_i^{J,M}$ calculated with these values for the helicity amplitudes. Hence, with the restriction to the lowest multipole, the angular distributions of a χ_c decay for a given polarization state $|J, M\rangle$ is fully determined (obviously, the relative contributions of different polarization states are not fixed).

TABLE IX. Helicity density matrix for the J/ψ decay as defined in J/ψ decay as defined in (A2).

$\sigma \setminus \sigma'$	-1	0	1
-1	$\frac{1+\cos^2\theta'}{2}$	$-\frac{\sin\theta' \cos\theta'}{\sqrt{2}} e^{i\phi'}$	$\frac{\sin^2\theta'}{2} e^{2i\phi'}$
0	$-\frac{\sin\theta' \cos\theta'}{\sqrt{2}} e^{-i\phi'}$	$\sin^2\theta$	$\frac{\sin\theta' \cos\theta'}{\sqrt{2}} e^{i\phi'}$
1	$\frac{\sin^2\theta'}{2} e^{-2i\phi'}$	$\frac{\sin\theta' \cos\theta'}{\sqrt{2}} e^{-i\phi'}$	$\frac{1+\cos^2\theta'}{2}$

TABLE X. The angular distribution terms $T_i^J(\theta, \theta', \phi')$ and the coefficients $K_i^{J,M}(A_{|\nu|})$ as defined in (A3) for $J = 1, 2$. The last columns give the numerical values for the coefficients $K_i^{J,M}$ for different M with the assumption that only the electric dipole transition contributes [see (A5)].

$J = 1$								
i	T_i^1	$M = 0$		$M = 1$				
		$K_i^{1,M}$ (general)						
		$M = 0$		$M = 1$		$K_i^{1,M}$ (E1 only)		
1	1	A_1^2		$\frac{1}{2}(A_0^2 + A_1^2)$		0.5		
2	$\cos^2\theta$	$A_0^2 - A_1^2$		$\frac{1}{2}(-A_0^2 + A_1^2)$		0		
3	$\cos^2\theta'$	$-A_1^2$		$\frac{1}{2}(A_0^2 - A_1^2)$		-0.5		
4	$\cos^2\theta\cos^2\theta'$	$A_0^2 + A_1^2$		$-\frac{1}{2}(A_0^2 + A_1^2)$		1.0		
5	$\sin 2\theta \sin 2\theta' \cos\phi'$	$-\frac{1}{2}A_0A_1$		$\frac{1}{4}A_0A_1$		-0.25		
$J = 2$								
i	T_i^2	$M = 0$		$M = 1$		$M = 2$		
		$K_i^{2,M}$ (general)						
		$M = 0$		$M = 1$		$M = 2$		$K_i^{2,M}$ (E1 only)
1	1	$\frac{1}{4}A_0^2 + \frac{3}{8}A_2^2$		$\frac{1}{2}A_1^2 + \frac{1}{4}A_2^2$		$\frac{3}{8}A_0^2 + \frac{1}{2}A_1^2 + \frac{1}{16}A_2^2$		0.25
2	$\cos^2\theta$	$-\frac{3}{2}A_0^2 + 3A_1^2 - \frac{3}{4}A_2^2$		$\frac{3}{2}A_0^2 - \frac{3}{2}A_1^2$		$-\frac{3}{4}A_0^2 + \frac{3}{8}A_2^2$		0.3
3	$\cos^4\theta$	$\frac{9}{4}A_0^2 - 3A_1^2 + \frac{3}{8}A_2^2$		$-\frac{3}{2}A_0^2 + 2A_1^2 - \frac{1}{4}A_2^2$		$\frac{3}{8}A_0^2 - \frac{1}{2}A_1^2 + \frac{1}{16}A_2^2$		-0.45
4	$\cos^2\theta'$	$\frac{1}{4}A_0^2 + \frac{3}{8}A_2^2$		$-\frac{1}{2}A_1^2 + \frac{1}{4}A_2^2$		$\frac{3}{8}A_0^2 - \frac{1}{2}A_1^2 + \frac{1}{16}A_2^2$		0.25
5	$\cos^2\theta\cos^2\theta'$	$-\frac{3}{2}A_0^2 - 3A_1^2 - \frac{3}{4}A_2^2$		$\frac{3}{2}A_0^2 + \frac{3}{2}A_1^2$		$-\frac{3}{4}A_0^2 + \frac{3}{8}A_2^2$		-1.5
6	$\cos^4\theta\cos^2\theta'$	$\frac{9}{4}A_0^2 + 3A_1^2 + \frac{3}{8}A_2^2$		$-\frac{3}{2}A_0^2 - 2A_1^2 - \frac{1}{4}A_2^2$		$\frac{3}{8}A_0^2 + \frac{1}{2}A_1^2 + \frac{1}{16}A_2^2$		1.35
7	$\sin^2\theta' \cos 2\phi'$	$-\frac{\sqrt{6}}{4}A_0A_2$		0		$\frac{\sqrt{6}}{8}A_0A_2$		-0.15
8	$\cos^2\theta\sin^2\theta' \cos 2\phi'$	$\frac{\sqrt{6}}{4}A_0A_2$		$-\frac{\sqrt{6}}{2}A_0A_2$		0		0.6
9	$\cos^4\theta\sin^2\theta' \cos 2\phi'$	$-\frac{3\sqrt{6}}{4}A_0A_2$		$\frac{\sqrt{6}}{2}A_0A_2$		$-\frac{\sqrt{6}}{8}A_0A_2$		-0.45
10	$\sin 2\theta \sin 2\theta' \cos\phi'$	$\frac{\sqrt{3}}{4}A_0A_1 + \frac{3\sqrt{2}}{8}A_1A_2$		$-\frac{\sqrt{3}}{4}A_0A_1$		$\frac{\sqrt{3}}{8}A_0A_1 - \frac{3\sqrt{2}}{16}A_1A_2$		0.3
11	$\cos^2\theta \sin 2\theta \sin 2\theta' \cos\phi'$	$-\frac{3\sqrt{3}}{4}A_0A_1 - \frac{3\sqrt{2}}{8}A_1A_2$		$\frac{\sqrt{3}}{2}A_0A_1 + \frac{\sqrt{2}}{4}A_1A_2$		$-\frac{\sqrt{3}}{8}A_0A_1 - \frac{\sqrt{2}}{16}A_1A_2$		-0.45

- [1] T. Matsui and H. Satz, Phys. Lett. B **178**, 416 (1986).
 [2] R. V. Gavai *et al.*, Int. J. Mod. Phys. A **10**, 3043 (1995).
 [3] R. Baier and R. Rückl, Z. Phys. C **19**, 251 (1983); G. A. Schuler, CERN Report No. CERN-TH.7170/94.
 [4] G. T. Bodwin *et al.*, Phys. Rev. D **51**, 1125 (1995); M. Beneke and I. Z. Rothstein, Phys. Rev. D **54**, 2005 (1996); **54**, 7082(E) (1996).
 [5] C. Amsler *et al.*, Phys. Lett. B **667**, 1 (2008).
 [6] R. Vogt, Nucl. Phys. A **700**, 539 (2002).
 [7] J. H. Cobb *et al.*, Phys. Lett. **72B**, 497 (1978).
 [8] A. G. Clark *et al.* (R702 Collaboration), Nucl. Phys. **B142**, 29 (1978).
 [9] C. Kourkoumelis *et al.*, Phys. Lett. **81B**, 405 (1979).
 [10] D. A. Bauer *et al.* (E610 Collaboration), Phys. Rev. Lett. **54**, 753 (1985).
 [11] L. Antoniazzi *et al.* (E705 Collaboration), Phys. Rev. Lett. **70**, 383 (1993).
 [12] F. Abe *et al.* (CDF Collaboration), Phys. Rev. Lett. **79**, 578 (1997).
 [13] T. Alexopoulos *et al.* (E771 Collaboration), Phys. Rev. D **62**, 032006 (2000).
 [14] T. Affolder *et al.* (CDF Collaboration), Phys. Rev. Lett. **86**, 3963 (2001).
 [15] I. Abt *et al.* (HERA-B Collaboration), Phys. Lett. B **561**, 61 (2003).
 [16] T. B. W. Kirk *et al.* (E369 Collaboration), Phys. Rev. Lett. **42**, 619 (1979).
 [17] Y. Lemoigne *et al.* (WA11 Collaboration), Phys. Lett. **113B**, 509 (1982); **116B**, 470(E) (1982).
 [18] F. Binon *et al.* (IHEP Collaboration), Nucl. Phys. **B239**, 311 (1984).
 [19] S. R. Hahn *et al.* (E673 Collaboration), Phys. Rev. D **30**, 671 (1984).
 [20] D. A. Bauer *et al.* (E610 Collaboration), Phys. Rev. Lett. **54**, 753 (1985).
 [21] L. Antoniazzi *et al.* (E705 Collaboration), Phys. Rev. Lett. **70**, 383 (1993).
 [22] V. Koreshev *et al.* (E672/706 Collaboration), Phys. Rev. Lett. **77**, 4294 (1996).
 [23] A. Sansoni *et al.* (CDF Collaboration), Il Nuovo Cimento A **109**, 827 (1996).
 [24] L. Gerland *et al.*, Phys. Rev. Lett. **81**, 762 (1998).
 [25] B. Alessandro *et al.*, Eur. Phys. J. C **39**, 335 (2005).
 [26] R. Arnaldi *et al.*, Nucl. Phys. **A774**, 711 (2006).
 [27] H. Buesching and H. Pereira da Costa, Nucl. Phys. **A774**, 747 (2006); O. Drapier, Nucl. Phys. **A774**, 325 (2006).
 [28] M. Nardi, Nucl. Phys. **A774**, 353 (2006).
 [29] I. Abt *et al.* (HERA-B Collaboration), Eur. Phys. J. C **49**, 545 (2007).
 [30] F. Maltoni *et al.*, Phys. Lett. B **638**, 202 (2006).
 [31] HERA-B, DESY Design Report No. DESY-PRC 95/01, 1995.
 [32] K. Ehret Nucl. Instrum. Methods Phys. Res., Sect. A **446**, 190 (2000).

- [33] C. Bauer *et al.*, Nucl. Instrum. Methods Phys. Res., Sect. A **501**, 39 (2003).
- [34] H. Albrecht *et al.*, Nucl. Instrum. Methods Phys. Res., Sect. A **541**, 610 (2005); **555**, 310 (2005); **576** 312 (2007).
- [35] I. Ariño *et al.*, Nucl. Instrum. Methods Phys. Res., Sect. A **516**, 445 (2004).
- [36] G. Avoni *et al.*, Nucl. Instrum. Methods Phys. Res., Sect. A **580**, 1209 (2007).
- [37] V. Eiges *et al.*, Nucl. Instrum. Methods Phys. Res., Sect. A **461**, 104 (2001).
- [38] I. Abt *et al.* (HERA-B Collaboration), Phys. Rev. D **73**, 052005 (2006).
- [39] M. Villa *et al.*, *Proceedings of VII International Conference on Calorimetry in High Energy Physics (CALOR 97)*, Tucson, AZ, 9–14 Nov 1997, edited by E. Cheu, T. Embry, J. Rutherford, and R. Wigmans (World Scientific, Singapore, 1998), p. 537.
- [40] T. Sjöstrand, Comput. Phys. Commun. **82**, 74 (1994).
- [41] H. Pi, Comput. Phys. Commun. **71**, 173 (1992).
- [42] R. Brun *et al.*, GEANT3, CERN Report No. CERN-DD-EE-84-1, 1987.
- [43] M. G. Olsson and C. J. Suchyta, Phys. Rev. D **34**, 2043 (1986); A. D. Martin, M. G. Olsson, and W. J. Stirling, Phys. Lett. **147B**, 203 (1984).
- [44] P. Faccioli (HERA-B Collaboration), Nucl. Phys. A **783**, e1 (2007); I. Abt *et al.* (HERA-B Collaboration), (unpublished).